Metallurgy

Joachim E. Hoffmann, Vrushali Pawar, Dietmar Eifler, Tina Eyrisch, Torsten Hielscher, Monika Saumer, Patrick Klär, Martin-Tobias Schmitt and Peter Starke*

Surface states by grinding thin strips of electrochemically deposited nanocrystalline nickel-iron

https://doi.org/10.1515/mt-2022-0015

Abstract: Thin strips of electrochemically deposited nanocrystalline nickel-iron with thicknesses of 320 or 330 µm are modified by defined grinding. Small changes in the cutting depth and the variation of the grinding process, up cut or down cut, result in different surface states. X-ray diffraction provides the analyses of the microstructures and residual stresses on the surfaces. In the initial state, the grain sizes have an average value of 9.3 nm, the micro strains 0.74% and the residual stresses predominantly values in the low-pressure range. Up grinding with the smallest depth of cut 1 µm causes the lowest compressive residual stresses at workpiece surface due to cold plastic deformation. Larger cutting depths and surface temperatures reduce the mechanical effects. Then prevailing thermal effects cause tensile residual stresses through thermoplastic deformation and through changes in the microstructure, which can be observed by grain enlargements and decreases in micro strains. However, the recovery and recrystallization processes are only partial. Down grinding with a cutting depth of 3 µm thus leads to a maximum grain size increase to 23.4 nm and a maximum decrease in micro strain to 0.41% as well as to maximum residual stresses of 880 MPa.

Keywords: electrodeposition; microstructure; nanocrystalline nickel-iron; roughness; X-ray diffraction.

1 Introduction

Material surface and/or edge layer states of conventional microcrystalline (mc, grain size $D > 1$ µm) metals are defined by mechanical [1, 2] as well as by thermochemical or thermal [3, 4] edge layer treatment methods for different properties. Local changes in the residual stresses, the strain hardening (e.g. dislocations and twin density), the structure state, the component topography state, changes in component geometry (distortion), as well as cracks as a result of unfavorable process parameters occur. On microcrystalline metals, such conditions have been systematically investigated and optimized for some time to improve the strength and other properties of components [3–7]. Residual stresses can significantly influence the mechanical properties of a component.

Residual stresses are defined as mechanical stresses in components without external loads and moments and without temperature gradients [8, 9]. The associated internal forces and moments are in mechanical equilibrium. According to their homogenous extension (constant absolute value and constant direction) they can be differed in residual stresses type I, II, and III. Residual stresses type I are almost homogenous over larger material areas (several grains), residual stresses type II in rather small areas (grain or grain ranges), whereas residual stresses type III are inhomogeneous over some atomic distances. The locally effective residual stress state results from the superposition

***Corresponding author: Peter Starke**, Materials Science and Materials Testing, Institute QM[3], University of Applied Sciences Kaiserslautern, Schoenstraße 11, 67659 Kaiserslautern, Rheinland-Pfalz, Germany, E-mail: peter.starke@hs-kl.de
Joachim E. Hoffmann, Vrushali Pawar and Martin-Tobias Schmitt, Materials Science and Materials Testing, Institute QM[3], University of Applied Sciences Kaiserslautern, Schoenstraße 11, Kaiserslautern, Rheinland-Pfalz, Germany
Dietmar Eifler, Institute of Materials Science and Engineering, TU Kaiserslautern University, Kaiserslautern, Rheinland-Pfalz, Germany
Tina Eyrisch, Institute QM[3], University of Applied Sciences Kaiserslautern, Schoenstraße 11, Kaiserslautern, Rheinland-Pfalz, Germany
Torsten Hielscher, Manufacturing Technology, Institute QM[3], Hochschule Kaiserslautern, Schoenstraße 11, Kaiserslautern, Rheinland-Pfalz, Germany
Monika Saumer, Chemical Processes in Microsystems Technology, University of Applied Sciences Kaiserslautern, Amerikastraße 1, Zweibrücken, Rheinland-Pfalz, Germany
Patrick Klär, Microsystems Design and Simulation, University of Applied Sciences Kaiserslautern, Amerikastraße 1, Zweibrücken, Rheinland-Pfalz, Germany

of the residual stresses type I, II and III. This classification is also very suitable for X-ray analysis. Subsequently, the stresses measured from the displacement of the X-ray interference lines are referred to as residual stresses. These are residual stresses type I, type I and II, or only type II. The micro strains or residual stresses type III can be derived from the widening of the X-ray interference lines.

Specifically carried out mechanical edge layer treatments, such as shot peening, deep rolling, or grinding, causes a considerable increase of the fatigue strength due to compressive residual stresses of sufficient penetration depth [3–7]. Preconditions are material states with higher hardness or strength as well as inhomogeneous stresses, e.g. bending or notch effects. High compressive residual stresses and high edge hardness result in high local fatigue strengths in the highly stressed edge area. The local fatigue strength must exceed the local stress at each coordinate of the component. The associated significant increase in component fatigue strength can completely cancel out the notch effect. Tensile residual stresses after grinding of high or higher-strength materials with unfavorable grinding parameters, on the other hand, lead to a sharp decrease in fatigue strength. The situation is different for materials of lower strength. These show a reduction of the manufacturing-related residual stresses under cyclic component stress with sufficiently high plastic deformations. Residual stresses are thus virtually without influence on the fatigue behavior. In addition, rough surface topographies can reduce the fatigue strength of components [5, 10]. Surface qualities with low roughness values must therefore be generated, especially for materials with higher strength.

2 Theoretical approach

Grinding is one of the chip removing mechanical edge layer treatment methods. The focus is on the design and the production of high surface qualities with small surface roughness. Tensile residual stress on the workpiece surface has to be avoided. The formation of residual stresses during grinding is essentially determined by the cutting power introduced into the material surface/edge zone, which depends on various grinding parameters [6, 11, 12]. Basically, elastic-plastic deformations occur in the near-surface areas due to the contact between the tool and workpiece during grinding, as with other residual stress-generating cutting processes. Larger temperature changes and structural transformations may develop. Mechanical and thermal processes therefore occur simultaneously during the grinding process. These are assessed in a scheme [13–15]. Low cutting power or depth of cut cause compressive residual stresses due to cold plastic squeezing processes. With an increase in cutting power, heat generation predominates. Higher temperatures then lead to thermal expansion of the surface layer at the material surface and thermal plastic compression due to the underlying cold material area when reaching the warm yield strength. After the grinding wheel has been moved on and the surface layer has cooled down, there are tensile residual stresses that can even produce surface cracks if the amounts are too high. Structural changes such as e.g. martensite formation in hardenable steels and compressive residual stresses are also possible. Key influencing factors and the development processes of residual stresses in the grinding of metallic materials are more closely considered in a recent overview [16].

The cutting power, the depth of cut and other grinding parameters such as the use of cooling lubricant (type, quantity, supply, pressure), the cutting speed and workpiece speed, up or down grinding, the type of grinding wheel, the wear and the dressing conditions of the grinding wheel, as well as the workpiece material, the shape of the workpiece and the machining direction result in more or less strong differences in the near-surface residual stresses. For example, when grinding steel with CBN, much less heat is introduced into the workpiece than with Corundum or SiC discs [11, 12, 17]. Therefore, and because of the better wear resistance, CBN grinding wheels usually generate compressive residual stresses in the near-surface area. Ceramic abrasives lead to absolutely higher residual stresses than CBN at the same grinding parameters. Surface tensile residual stresses may already be present after grinding with lower depths of cut. Grinding with CBN also leads to lower surface roughness and higher surface hardness.

Down or up grinding of steel with a depth of cut of 20 μm with the use of a cooling lubricant show practically no differences in surface residual stresses. But for dry grinding, there are higher compressive residual stresses in down grinding than in up grinding [18]. However, creep feed grinding tests with low material removal rate lead to higher temperatures in the contact zone and the newly generated surface when down grinding compared to up grinding [19]. For larger material removal rates, it is reversed on the generated surface. In this case, higher temperatures are measured for up grinding than for down grinding. In the further contact zone, however, higher temperatures are present in down grinding than in up grinding.

The grinding direction and the feed direction, respectively, must also be taken into account with regard to the formation of residual stresses. On smooth workpiece surfaces there are usually absolutely higher values of the

near-surface residual stresses in the machining direction than across it [5, 14, 20]. Notched workpiece surfaces show similar dependencies on the above mentioned grinding parameters [15, 21, 22]. However, smaller amounts of surface tensile and compressive residual stresses are usually measured in the notch direction as well as the machining direction than transversely.

The hardening and the by X-ray determined half-width value in the surface layer respectively increases when grinding steel in normalized and tempered condition [5, 14, 15, 21]. In hardened condition, on the other hand, the hardening can increase or decrease during grinding. The causes are changes in dislocation density and microstructure. The impact depth of the affected surface layer is rather small for grinding. It is in the hundredth to the tenth of a millimeter range.

The influences of the grinding parameters on the material surface states produced are confirmed for nickel-based alloys with a microcrystalline microstructure. Processes of plastic deformation and heat development are decisive. For example, pendulum grinding of the alloy GH4169 is carried out with a ceramic grinding wheel by varying the depth of cut from 5 to 40 µm. Increasing in depth of cut leads to an increase in grinding temperatures and thus in surface tensile residual stresses, namely in the grinding direction from 700 to around 1100 MPa and in the transverse direction from around 540 to 930 MPa [23]. The surface roughness increases significantly. In addition, the micro-hardness decreases with increasing depth of cut. The impact depth of the decrease in hardness near the surface increases. This is caused by high grinding temperatures and associated structural changes. γ′ or γ″ – precipitations dissolve, larger grains are formed and the material near the surface is softened. The depth of the plastically deformed layer near the surface and the orientation of the grains in the grinding direction increase. With a depth of cut of 40 µm, the high tensile residual stresses exceed the material strength and cracks appear perpendicular to the grinding direction. Low grinding temperatures are assumed for very low depth of cut, sharp abrasive grains, and good cooling lubrication. Plastic deformation dominates, the material is hardened, and surface compressive residual stresses arise. In the case of the nickel-based superalloy K417, with increasing depth of cut, increasing absolute residual stresses or decreasing compressive residual stress amounts are measured due to higher temperatures [24].

Creep feed grinding of nickel-based superalloy IN738LC results in medium to high tensile residual stresses for differently dressed ceramic grinding wheels [25]. Very unfavorable conditions, such as grinding without coolant, can result in local initial melts and white layers with nanocrystalline microstructures, very high tensile residual stresses of up to 1850 MPa and cracks on the workpiece surface. However, CBN grinding wheels with coolant produce surface residual stresses close to zero. Reasons are the good thermal conductivity of CBN and thus the relatively lower workpiece surface temperatures. Ceramic and CBN grinding wheels provide compressive residual stresses beneath the surface, with the exception of grinding with ceramic wheels without cooling.

Due to their mechanical, soft magnetic and chemical properties, nickel as well as nickel alloys are among the materials chosen for the production of layers as well as for smallest structures for micro electrical mechanical systems (MEMS), such as micro gears [26–28]. The manufacturing of high-precision micro-components is made by electrochemical deposition using LIGA technology or the direct-LIGA process [29]. Due to their nanocrystalline (nc) microstructure with grain sizes D < 100 nm, electrochemically deposited micro-components or layers have excellent mechanical properties [30–33]. The hardness and strength values are 2–10 times higher than for conventional microcrystalline (mc) materials with grain sizes in the µm range (grain size $D > 1$ µm).

Electrochemical metal deposition offers many process parameters to influence the microstructure (chemical composition, grain size, grain structure, twin density, textures), the residual stresses and micro strains, as well as the material properties of layers or micro-components in a defined manner. These influencing parameters include the bath composition, the bath process parameters, the set current parameters, the substrate and the structural geometry [27, 28, 30, 33–35]. LIGA micro-components show local irregularities in the current density, the electrolyte composition, the microstructure and the local properties. The edges or side edges of the micro-components usually grow the fastest because this is where the highest current densities prevail. In addition, alloys can have different compositions over the height of growth [28, 36]. In comparison, electrochemically deposited layers have a more uniform microstructure.

The grain size of electrodeposited Ni layers decreases as the current density increases, at first considerably, from the ultra-fine crystalline range (ufg, grain sizes 100 nm < D < 1000 nm) of around 200 nm at 1 A × dm^{-2} to the nanocrystalline (nc, D < 100 nm) range to 50 to 20 nm at 5 A × dm^{-2}. For higher current densities, from around 8 A × dm^{-2} to 30 A × dm^{-2}, the grain size remains constant at 25 to 20 nm [34]. Nickel-iron alloys behave in reverse. Here, the grain size increases slightly from 13 to 17 nm or 6 to 17 nm with the current density from 6 to 15 A × dm^{-2} or 0.2 to 10 A × dm^{-2} [27, 32, 33]. With the same current density, NiFe layers have smaller grains than Ni layers. Iron also

being deposited has a grain-refining effect [37, 38]. The reason is a higher nucleation rate for NiFe than for Ni. With increasing current density, however, the iron content in front of the deposition layer in the electrolyte and thus the number of nucleations decreases and the grain size increases. Compared to direct current deposition, pulsed current deposition offers many more process parameters that can influence the microstructure over a wide range. For example, short pulse durations in the millisecond range allow higher current densities than direct current deposition. Smaller grains below 20 nm are possible with short pulse durations and high current densities [30]. The additives used also reduce the grain size and increase the micro strain [30, 39, 40].

Sulfur-containing bath additives, such as saccharin, serve in small quantities as grain refiners and as brighteners in the deposition of nickel as well as nickel-iron layers [32, 35, 41–44]. In addition, they reduce or avoid the formation of tensile residual stresses and cracks. Fiber textures are formed within the layers. The addition of saccharin changes a distinct <200> fiber texture into a double fiber texture <111> and <200> [32, 33, 35, 39, 40, 43].

The residual stress development of nickel as well as nickel-iron or iron-nickel layers deposited electrochemically on the substrate depends on the many process parameters [41, 45–50]. For example, the deposition of nickel without saccharin provides tensile residual stresses, usually below 200 MPa [47]. For very small layer thicknesses of 0.5–1 µm, tensile residual stresses of around 140–350 MPa are obtained [44, 51, 52]. With increasing layer thickness of 10–20 µm, the tensile residual stresses decrease to around 100 MPa and then remain approximately constant. Depending on the substrate and the starting layer, nickel-iron layers form higher tensile residual stresses after the deposition of small layer thicknesses [41]. For Ni-21 wt% Fe with a deposited layer thickness of 0.5 µm, e.g., residual stresses up to 450 MPa are obtained. From a layer thickness of 2 and 5 µm, the tensile residual stresses drop down to 150 and 100 MPa, respectively. Iron-nickel layers, also deposited without saccharin, have very high tensile residual stresses of more than 1000 MPa for very thin layers < 2 µm [46]. As the layer thickness growths to 10 µm, the tensile residual stresses decrease to below 200 MPa and show only small changes for a further increase of the layer thickness.

The current density is one of the most important process parameters for the arising of residual stresses and the microstructure formation within the layers. In nickel layers for additive-free deposits, low current densities produce low tensile residual stresses and higher current densities generate higher tensile residual stresses [43, 44, 47, 49, 53]. This means, in nickel layers, the absolute values of the residual stresses increase and the grain sizes decrease with the current density. Saccharin, on the other hand, forms smaller residual stresses in very fine grains in terms of absolute values. Nickel layers deposited with or without saccharin show considerable differences in the absolute residual stress values of –842 or –143 MPa and the grain sizes of 10 or 5000 nm [48]. This is different with the alloying of iron in nickel. Compared to pure nickel deposits, the nickel-iron alloy Ni-16 wt% Fe has smaller grain sizes of 12 vs. 23 nm, but absolutely higher residual stresses of –2 vs. –70 MPa [50]. Smaller nc grains or higher iron contents also show higher micro strains [32, 33, 43]. Increasing iron contents in the NiFe layers, adjusted by means of the current density and/or the bath composition, even when using the additive saccharin, result for up to about 15 wt% Fe in decreasing compressive residual stresses and for up to 50 wt% Fe even high tensile residual stresses of up to 700 MPa [41]. In addition, various other process parameters, such as further bath additives, the pH value, the pulse current and its parameters, different stirring, the temperature and pressure of the electrolyte or the type of substrate, have more or less effects on the microstructure formed, the texture, the residual stresses, the micro strains, the surface roughness and thus the mechanical properties [35, 41–43, 47, 48, 52, 53].

For the formation of residual stresses in deposited layers on substrates, in addition to thermal residual stresses, various causes, theories and models are mentioned in the literature [50, 52]. Most theories deal with changes of the deposition volume such as the coalescence of crystallites, the inclusion of hydrogen or other foreign substances, the generation of lattice defects or lattice misfits between layer and substrate. Furthermore, the effects of excess energies compared to the equilibrium state are considered [54]. The coalescence theory, for example, explains the formation of tensile residual stresses or increasing residual stresses in nickel or NiFe or FeNi layers for grains smaller than 100 nm with the fact that the contraction caused by the attractive forces of the deposited very small crystals is hindered due to the bond to the substrate [41, 45, 50, 52]. Smaller grains and thinner layers have higher tensile residual stresses [45, 50]. For thicker layers, from 0.5 µm, a decreasing proportion of coalescence and hence other causes for the formation of residual stresses are assumed [45]. Further arguments suggest that coalescence cannot be viewed as the origin of residual stresses in polycrystalline layers, but only as an additional factor that can change the free surface energy of the crystallites [54].

According to a model called general thermodynamic theory, the residual stresses are calculated according to the deviation of the nc grains from thermodynamic

equilibrium or the excess of free surface and grain boundary energy [54]. The considerations deal with the initial stages of the electrochemical deposition before the coalescence of the individual crystals, as well as with influences of the coalescence, the additives, the bath composition, the thickness of the deposition layer, the current density and the bath temperature. Depending on the deviation from the equilibrium shape and size of the crystals, tensile or compressive residual stresses can be determined. The grain refinement with saccharin is due to its almost complete closure of the {111} planes on the cathode surface caused by the formation of complex compounds [35, 43]. On the remaining free surface parts, the current density at the cathode and hence the rate of nucleation increases and the surface diffusion of the nickel ions decreases [35, 52]. Altogether this results in finer grains as the lateral crystal growth decreases. The {111} planes can develop perpendicular to the free surfaces at the expense of the {200} planes. The corresponding change in texture, the deviation of the crystal shape and size from the equilibrium case, and the coalescence lead to the formation of compressive residual stresses [43, 54].

The increase or decrease in volume due to the inclusion of foreign atoms provides an additional explanation for the formation of compressive or tensile residual stresses in nickel layers [52]. Saccharin and its deposition of complex compounds at the grain boundaries cause an increasing volume and compressive residual stresses. As a further example, according to a hydrogen theory, metal hydrides or metal hydroxides are formed during the deposition process, which require larger volumes in the lattice, but are not stable and decompose [43, 54]. The hydrogen diffuses out of the layer. The remaining metal ions require less volume. A contraction of the lattice with tensile residual stresses occur. In addition, the adsorption of hydrogen in the nickel layer can act as a grain refiner similar to saccharin.

Thermal residual stresses are rather small, but can also be larger depending on the respective process parameters [35, 41, 47, 49, 51, 52, 54]. They result from the difference in the thermal expansion coefficients of the layer and substrate material as well as from the temperature difference between the bath temperature during the electrochemical deposition and the ambient temperature.

Micro strains or lattice expansions as local inhomogeneous strains are the result of generated local errors, such as dislocations, vacancies, twins, foreign atoms or grain boundaries. They are also influenced by the process parameters of the electrochemical deposition. Increasing current density in pure nickel layers leads to decreasing grain sizes and increasing micro strains [40]. In the case of nickel-iron alloys, higher current densities or appropriate bath compositions produce decreasing iron contents, increasing grain sizes and thus decreasing micro strains [32, 33, 38].

The determination of residual stresses on the electrochemically deposited layers usually takes place in the compound of substrate and layer [41–44, 46–53]. For this purpose, mainly mechanical methods are used [41, 43, 44, 46, 47, 49–53, 55]. From the measured deformations of bending strips coated on one side (bend strip method) or the torsion of spiral contractometers or the deflections of discs or AFM cantilevers as well as the axial elongation or shortening of thin strips coated on both sides (strip stretching method, change of length) the averaged residual stresses of the respective layer are determined [41, 43, 44, 46, 51, 52, 55, 56]. The bending strip method is considered to be best suited for industrial practice because it allows sufficient accuracy and quick results at low cost. Another advantage of the mechanical methods is that the residual stresses can be determined continuously during the layer growth.

By means of the X-ray diffraction method (XRD) the internal stresses can be determined locally and directly on the layer or on the micro-component with an adequately high lateral resolution [41, 42, 48]. The stress distribution and the crystalline structure from the layer surface to layers close to the substrate can be determined. In simplified terms, the X-ray stress analysis is carried out by measuring the displacement of the X-ray interference lines or the lattice strains of a certain type of lattice plane at different tilt angles ψ. For linear line position distributions versus $\sin^2\psi$, residual stresses are obtained from a straight line slope using the $\sin^2\psi$ method [57]. Also for nc nickel or nc nickel alloys linear line position distributions are evaluated [41, 42, 48]. However, for very thin nickel layers, below 4 µm, the classical $\sin^2\psi$ method for the determination of residual stresses could not be applied [58]. Too low intensities of the interference lines after subtraction of the background and a relatively high, inconsistent impact depth of the X-rays are the reason for difficulties during measurement. This can be remedied by X-ray diffractometry with low angles of incidence (low-incident-beam-angle diffraction technique). Difficulties in the evaluation can also arise due to the texture [59]. Thicker layers of around 4 µm show linear line position distributions over $\sin^2\psi$ [58].

Electrochemical deposition of nc nickel alloys as layers or as high-precision direct-LIGA micro-components and their post-processing to exact thickness dimensions should show high surface quality, low distortion and thus mostly low residual stresses as well as good mechanical, chemical

or physical properties. High fatigue strength values can be achieved in particular due to the nc microstructure [60]. Work hardening as in the cold rolling of C-2000 (Hastelloy) can also contribute to a high fatigue strength [61]. In numerical simulations, however, compressive residual stresses show little effect on fatigue strength [61]. Nevertheless, results on nickel layers, deposited electrochemically on steel, show a clear influence of residual stress on the fatigue strength [47]. It can probably be assumed that for nanocrystalline as well as for microcrystalline metals, compressive residual stresses have a positive effect and tensile residual stresses have a negative influence on the fatigue strength. However, precise evaluations of the influence of residual stresses on the fatigue strength of nanocrystalline metals can only be carried out under difficult conditions [60]. This is justified with the simultaneous change of several layer states (e.g. the structure as grain size, alloy content, and texture or the residual stresses) in the case of electrochemical deposition, even if only one process parameter (e.g. the current density) is varied. Clear statements would require the separate consideration of the structural parameters, the micro-hardness, the residual stresses and the surface topography.

In the present work, the electrochemical deposition of nc nickel-iron layers on copper rounds is carried out, for material states as constant as possible with constant process parameters. Subsequent cutting and careful grinding might provide thin layer strips of high surface quality and high accuracy with a small thickness of only 320 or 330 µm. Different conditions close to the surface can be set with varied grinding parameters. The microstructure, residual stresses, micro strains, surface topographies and layer thicknesses obtained are recorded by X-ray and other analysis methods. The aim is to gain knowledge about the grinding of varied material and manufacturing/residual stress states on the surface of thin layer strips made of nc nickel-iron. The reason for thin layer strips is that they can be used to produce small samples or microsamples for subsequent fatigue tests.

3 Experimental procedure

The electrochemical deposition of nickel-iron layers occurs in two batches at a manufacturer of microdrives on copper rounds with a diameter of 99 mm and a thickness of 0.5 mm (Figure 1). An industrial electrolyte (pH = 3) with saccharin specially developed for microsystem technology is used [33]. The deposition takes place at a direct current (DC) density of $3\ A \times dm^{-2}$, resulting in a yield strength of at least 1700 MPa. Nickel-iron layers with a diameter of 89 mm and different thicknesses from 1.4 to 1.7 mm (Batch 1) or 1.8 to 3 mm (Batch 2) are produced. Differences in the thickness of the individual layers can be attributed to the electrochemical deposition, which is also different in the edge area compared to the middle of the layers. Eight coated rounds from the two batches are available: Batch 1: R032, R034, R036 and Batch 2: R038, R039, R042, R043, R044 (round numbers). Twelve layer strips with the dimensions 30 mm × 10 mm can be cut out of each of the rounds (Figure 1). To be able to clearly assign the position of the nickel-iron layer strips, a layout plan is needed (Figure 1). The designation of the layer strips consists of three parts. "R0xy" indicates the round number, the second digit "1 to 4" the quadrant number and third digit the position within a quadrant, ascending from "1 to 3" from inside to outside. In order to differentiate between the nickel-iron alloy side and the copper side during processing, a chamfer is applied to each layer strip in addition to the numeration. For grinding, the slightly bend layer strips require three M3 threaded holes to screw them flat on a specimen carrier. Desired essential geometric dimensions will be a uniform strip thickness h of 320 µm (Batch 1) or 330 µm (Batch 2), each with a tolerance of ± 10 µm (Figure 2a).

Cutting the rounds with a cutting machine (company: Buehler, type: PowerMet 3000) in four quadrants is the first step following the electrochemical deposition process. Subsequently, three layer strips are cut out of each

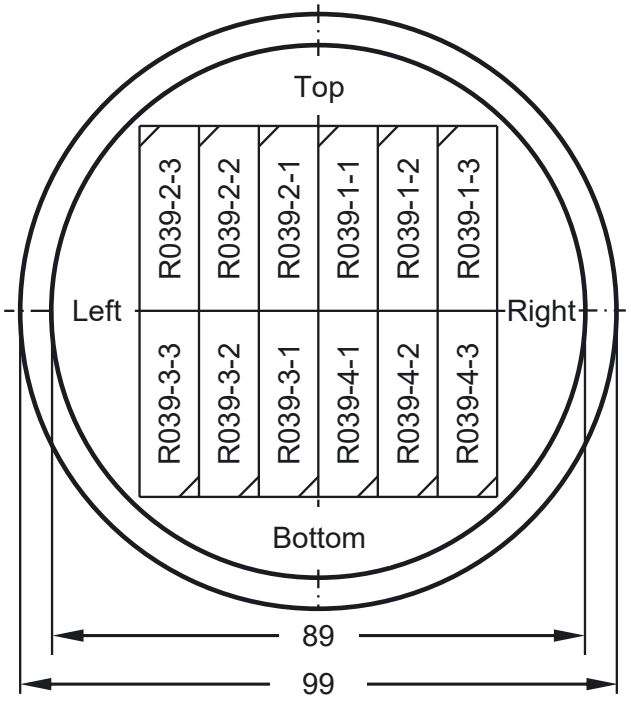

Figure 1: Positions of layer strips for nickel-iron coatings on a 99 mm diameter copper round.

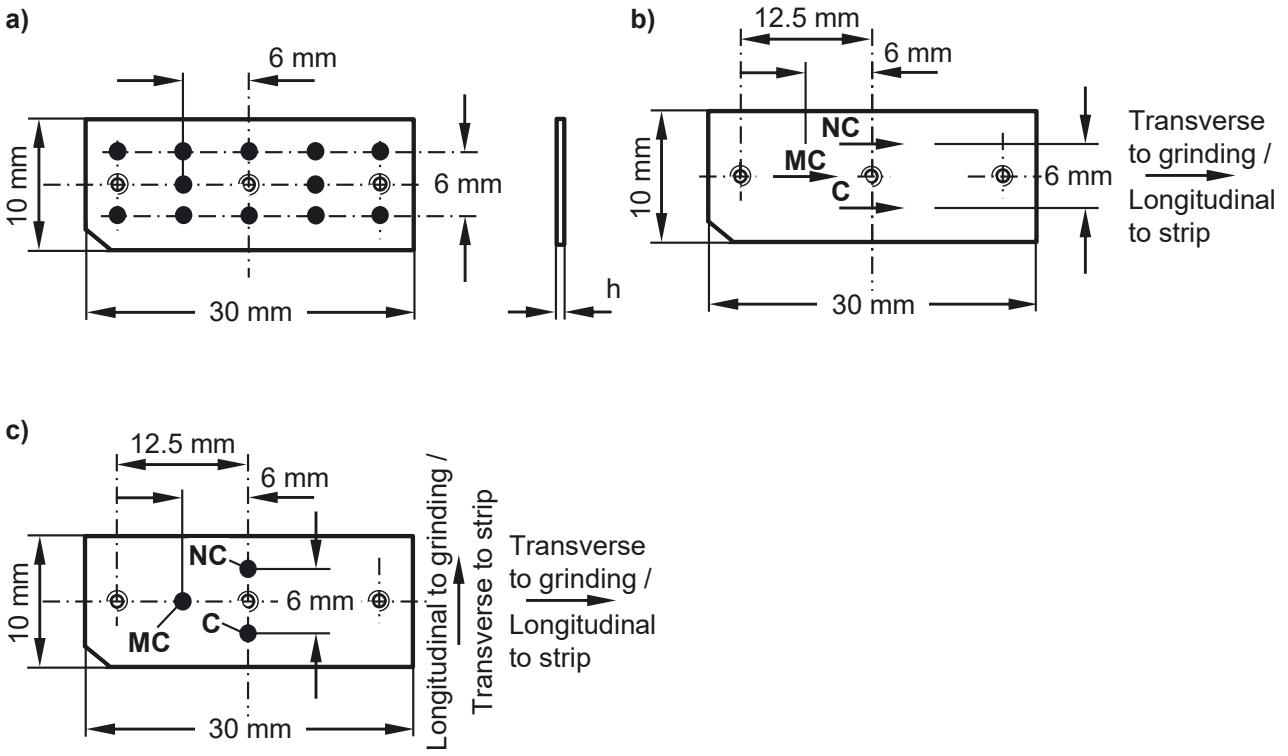

Figure 2: Strip geometry and a) positions for measuring strip thicknesses as well as C, NC and MC as b) lines for roughness measurements and as c) positions for X-ray diffraction analyses.

quadrant with a precision cutting machine (company: Struers, type: Accutom-50). Not all layer strips can be used for grinding because in some cases the nickel-iron layers have separated from the copper or because cracks have been developed during drilling or thread cutting.

Grinding is performed after further preparatory work and after positioning a specimen carrier with the fixed layer strip on the magnetic table of a surface grinding machine (company: Jung, type: Jutec 635). By using this setup, the varied depths of cut can be set in the µm range. The grinding tool for the further preparation is a silicon carbide ceramic grinding wheel with very fine grit (company: Lapport, type: SCG 220 G 9 V7500EF, Table 1).

Five grinding operations work off the layer strips on both sides down to a thickness of 320 (Batch 1) or 330 (Batch 2) µm. At the beginning, the grinding wheel is dressed and the specimen carrier with the layer strip screwed on the copper side is magnetically fixed on the grinding table. Pre-grinding means the first grinding process by pendulum movement of the grinding table (Table 1). The side of the strip with the nickel-iron layer is ground flat with a removal of 400 to 500 µm (Batch 1) or about 1200 µm (Batch 2). Secondly, the layer strip on the specimen carrier must be turned over to the other side. The grinding wheel is dressed again and 550 to 600 µm are ground off until all the copper is removed. In the third step, after dressing the grinding wheel again, the finish grinding follows on the former copper side removing 20 µm of nickel-iron by *N* identical passes with a depth of cut "a" in down grinding or up grinding (Table 1 and Figure 3). The fourth grinding process starts, after measuring the thickness of the strip, redressing the grinding wheel and turning the strip to the first NiFe side, as a further pre-grinding to a remaining thickness of 340 (Batch 1) or 350 (Batch 2) µm. Before finish grinding to strip thicknesses of 320 or 330 µm, the grinding wheel is dressed again (Table 1). In the fifth grinding process, again *N* equal passes with a depth of cut "a" are carried out in down grinding or up grinding for a removal of 20 µm.

Dressing before grinding, in particular before finish grinding, is important to reach defined surface states. This consistently works under the same conditions (except for strips of round R032), with sufficient material removal and sufficiently often (Table 1).

Grinding is performed transversely to the longitudinal axis of the strips (Table 1 and Figure 3). Only in the initial phase of the tests longitudinal grinding takes place on 12 strips of Batch 1 from round R032. Considering the

Table 1: Grinding process parameters and grinding wheel details.

Grinding wheel details	
Company	Lapport
Wheel model, material	SCG 220 G 9 V7500EF
Wheel width	40 mm
Wheel diameter	300 mm
Defined dressing of grinding wheel for all strips, except those of round R032	
Before each pre-grinding	3 × 20 µm
Before each finish grinding	3 × 20 µm
Grinding process parameters	
Specimen carrier	Fixing the strips for each grinding process
Cutting speed v_c	25 m × s^{-1}
Workpiece speed v_w	14 m × min^{-1}
Coolant	Emulsion
Grinding direction	Transverse, strips of Batch 1 and 2 Longitudinal, strips of round R032, Batch 1
Cross-feed	Deactivated, strips of Batch 1 and 2 Activated, strips of round R032, Batch 1
Pre-grinding	
Type of grinding method	Pendulum grinding
Depth of cut a	Automatic
Finish grinding	
Type of grinding method	Down or up grinding
N × depth of cut a	Very careful: 20 × 1 µm (smallest) Increased: 7 × 3 µm or 5 × 4 µm

geometry of the strips, 30 mm length, 10 mm width, and the thin strip thicknesses of 320 (Batch 1) or 330 µm (Batch 2), the low strip thicknesses in particular pose a challenge for finish grinding. Undesirable machining deformations of the thin strips should be less in transverse direction with the three times shorter width (10 mm) than in the longitudinal direction (30 mm). It therefore seems to be easier to reach more uniform surface states by grinding along the width of the strips, i.e. in the transverse direction.

Defined finish grinding with N passes × depth of cut a 20 × 1 or 7 × 3 or 5 × 4 µm is carried out without cross-feed. Grinding with cross-feed would not be unambiguous, since the previously created surface would be ground again without adjusted depth of cut. Therefore, no further grinding contacts than those of the set depths of cut N × a may arise in finish grinding. Exceptions are the strips of round R032, as this grinding uses cross-feed. Other parameters such as the cutting speed v_c or the workpiece speed v_w remain constant (Table 1).

To characterize the specimen fabrication, the measurement of the strip thickness h (Figure 2a) represents a first step. This must be done after each processing step. A micrometer screw gauge serves to measure the thickness at 12 points. Each point will be measured three times. The specified final thickness corresponds to the respective mean values of the strips.

Surface roughness measurements – as well as all other surface analyses – take place on the strips ground in the transverse direction. To get this realized, measurements are done along three lines of the finished strips (Figure 2b). These three measuring lines are placed in the middle (line MC) and near to the beginning or near to the end (line C, line NC) of the grinding path. Measuring direction is always perpendicular to grinding grooves or to grinding direction. To determine the measuring line length and to evaluate values for roughness depth R_z and arithmetic mean roughness R_a, measurements by using a confocal wide field microscope (company: Zeiss, type: Smart proof 5) with high resolution and high measuring speed are carried out according to standard DIN EN ISO 4287. For comparison and to ensure the accuracy of the roughness measurements, a stylus instrument, the Talysurf INTRA (company: Ametek, Taylor Hobson) is applied, confirming the results obtained with the confocal microscope.

The characterization of the nc microstructures as well as the residual stresses and micro strains on the surfaces of electrochemically deposited layer strips and on the surfaces of ground strips takes place by means of X-ray diffraction (XRD). A ψ -diffractometer (company: GE Sensing & Inspection Technologies GmbH, type: XRD 3003 PTS µB) can be used for this task. The Cu-Kα primary beam of a microfocus X-ray tube is gated for a lateral resolution of 200 µm in the center of the diffractometer with an X-ray light guide, an elliptical glass capillary (eFOX, Fiber Optic for X-rays). On the secondary side there is a semiconductor line detector (company: GE Sensing & Inspection Technologies GmbH, type: Meteor 1D) behind a nickel filter. It detects the Cu-Kα beam with a resolution of 50 µm, which previously diffracts at the lattice planes of the strips. Measurements are taken at points C, NC and MC (Figure 2c) transverse to the strip and therefore in the grinding direction as well as longitudinal to the strip and therefore transverse to the grinding direction (Figures 2c and 3a and 3b).

Grain sizes as well as micro strains are determined using the modified Williamson-Hall plot [62]. For this purpose, the respective interference line widths of the {311}, {222} and {400} lattice planes are to be measured. To verify the grain sizes determined by XRD, investigations on identical specimens with a transmission electron microscope (TEM) show

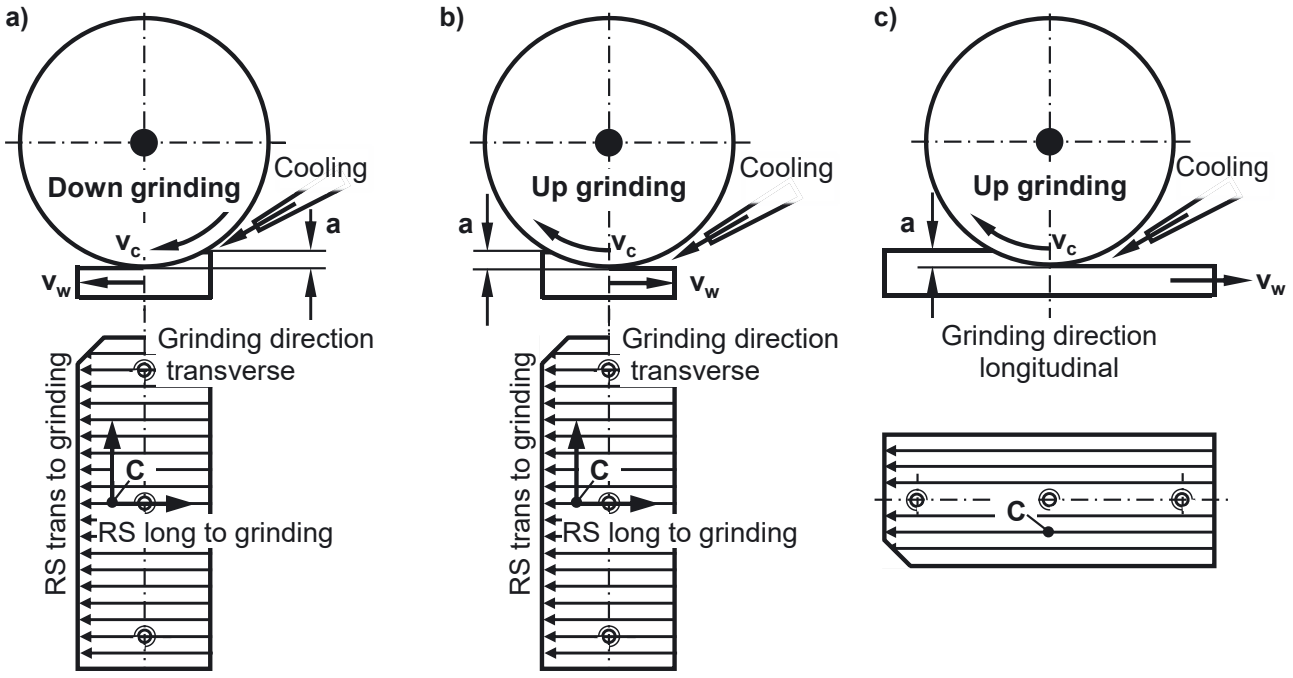

Figure 3: Schematic depiction as well as residual stress (RS) measurement direction longitudinal and transverse to transverse grinding of a) down and up grinding, b) transverse to strip, c) longitudinal to strip (v_c, cutting speed; v_w, workpiece speed; a, depth of cut).

the same results [32, 33]. The grain sizes determined by both methods were electrochemically deposited under the same conditions as for the microstructures considered here with direct current at 3 A × dm^{-2}.

XRD texture analyses of the lattice planes {111}, {200} and {220} can be performed for rotationally symmetrical pole figures using the relatively simple Harris texture index [63]

$$T_{\{hkl\}} = \frac{\frac{I^{mes}_{\{hkl\}}}{I^{rel}_{\{hkl\}}}}{\frac{1}{3}\left(\frac{I^{mes}_{\{111\}}}{I^{rel}_{\{111\}}} + \frac{I^{mes}_{\{200\}}}{I^{rel}_{\{200\}}} + \frac{I^{mes}_{\{220\}}}{I^{rel}_{\{220\}}}\right)} \quad (1)$$

evaluated respectively for constant azimuth angle φ = const. = 0° and for varied tilt angles ψ from ψ = 0° up to 70°. $I^{mes}_{\{hkl\}}$ and $I^{rel}_{\{hkl\}}$ are the measured and relative intensities of interferences from the NiFe specimens [64]. If an anisotropic microstructure is present, $T_{\{hkl\}}$ assumes a value greater than 1, and even up to a maximum of 3 if the texture is strongly pronounced. In the case of isotropic microstructures, $T_{\{111\}}$ = 1, $T_{\{200\}}$ = 1 and $T_{\{220\}}$ = 1.

Residual stress measurements are carried out on the {311} lattice planes with the Bragg angle $2\theta_0$ = 92.933° for nickel [65]. For further verification, the results of measurements on the {420} lattice planes at $2\theta_0$ = 155.675° are compared with those of the {311} lattice planes at $2\theta_0$ = 92.933° on the same strips and the same measurement points. Line position distributions with large tilt angle ψ range between −60° and +60° and equidistant $\sin^2\psi$ divisions of the 27 ψ -tilts provided good results. The residual stresses are obtained by the analysis of linear line position distributions according to the $\sin^2\psi$ method [57]. In the case of the {311} lattice planes the evaluation is based on a Young's modulus $E^{\{311\}}$ = 203,000 MPa and a Poisson's ratio $\nu^{\{311\}}$ = 0.32. In the comparison measurements, the diffraction-elastic constants of the {420} lattice planes coincide with those of the {311} lattice planes.

4 Results

The measured thickness values of the strips for nominal dimension 320 µm ± 10 µm tolerance (Batch 1) in Figure 4 reveal that only a defined, very careful grinding process can lead to the desired results (Table 1). However, almost all of the initial 12 longitudinally ground strips of round R032 with less suitable parameters are out of tolerance, sometimes with considerable deviations from the nominal value (Figure 4, left). Very carefully ground transversely to the longitudinal axis, with defined dressing of the grinding wheel, without cross-feed and with a very small depth of cut of 20 × 1 µm (Table 1), on the other hand, the thickness of each of the 10 strips is within the tolerance range (Figure 4, right). All these measured values have low

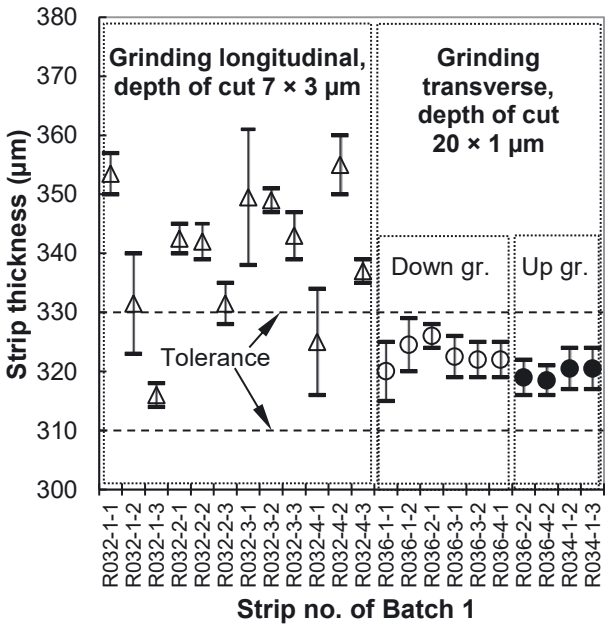

Figure 4: Strip thickness by grinding longitudinal (left) and by very careful grinding transverse (right) to the strips of Batch 1.

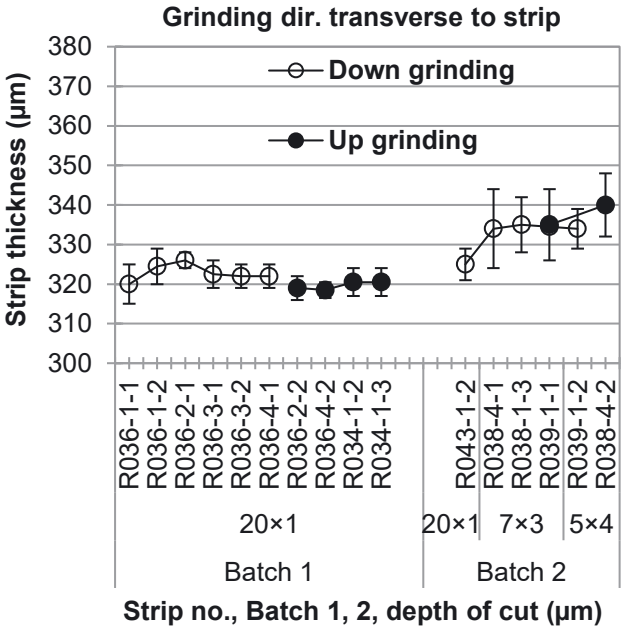

Figure 5: Strip thickness by transverse grinding with different depths of cut in down and up grinding of Batch 1 and 2.

scatter. Down and up grinding differ only slightly in the results.

In addition to Batch 1 (nominal value of thickness of 320 µm ± 10 µm tolerance), the nominal value of strip thickness of 330 µm for Batch 2 is slightly larger, likewise with ± 10 µm tolerance. Both batches show the lowest standard deviations of the strip thicknesses when grinding with the smallest depth of cut 20 × 1 µm (Figures 4 and 5). In comparison, larger depths of cut of 7 × 3 or 5 × 4 µm, as performed on Batch 2 strips, lead to larger standard deviations of the strip thicknesses. The mean values of the strip thicknesses of Batch 2 still fall within the tolerance, but the standard deviations exceed the upper tolerance limit 340 µm (Figure 5, right).

Roughness measurements, comparing the results of the two test devices, the confocal microscope and the stylus instrument, show practically no differences, determined on the same strips from Batch 2. On average, the value of R_z is 2.3 µm for Zeiss and 1.9 µm for Ametek. And for R_a, average values for Zeiss and Ametek of 0.25 and 0.27 µm respectively hardly differ. Apart from the nearly equal average values, the value of each strip is essentially the same. So all further roughness values are determined with the Zeiss Smart proof 5 confocal microscope.

Figure 6 shows results of roughness after finish grinding for the same strips as for thickness measurements (Figure 5). Roughness depth R_z is approximately the same for both down grinding (open symbols) and up grinding (closed symbols) as well as for Batch 1 and Batch 2 at about 2.1 µm (Figure 6a). It is observed that approximately equal roughness values R_z for lines C and NC at the beginning and the end of the grinding path remain slightly lower than those for line MC in the middle of the strips.

The arithmetic mean roughness value is on average for all measured strips of Batch 1 R_a = 0.41 µm and on average for all strips of Batch 2 R_a = 0.25 µm (Figure 6b). This means that the values for Batch 2 (with higher depths of cut) are one third smaller than those of Batch 1. As with R_z, the R_a between down and up grinding do not differ significantly when taking the measured values' scatter into account. Furthermore, R_a values on measurement lines MC in strip middle of Batch 1 are slightly larger than on measurement lines C and NC. This does not apply to Batch 2. Considered together, the R_a and R_z values do not fully correspond to results of a fine grinding process [10].

In electrochemically deposited state, surface residual stresses are measured at points C and NC along and transverse to the strip length (Figure 2c). The residual stresses of the coated strips of Batches 1 and 2 range in the low-pressure region or close to zero, with the exception of the strips from round R039 of Batch 2 (Figure 7). In most cases, there are no significant differences between points C and NC and between longitudinal and transverse directions. Nevertheless, the medium-sized compressive stresses of –314 to –110 MPa for R039-4-2 and R039-4-3 layer strips indicate differences in electrochemical deposition for

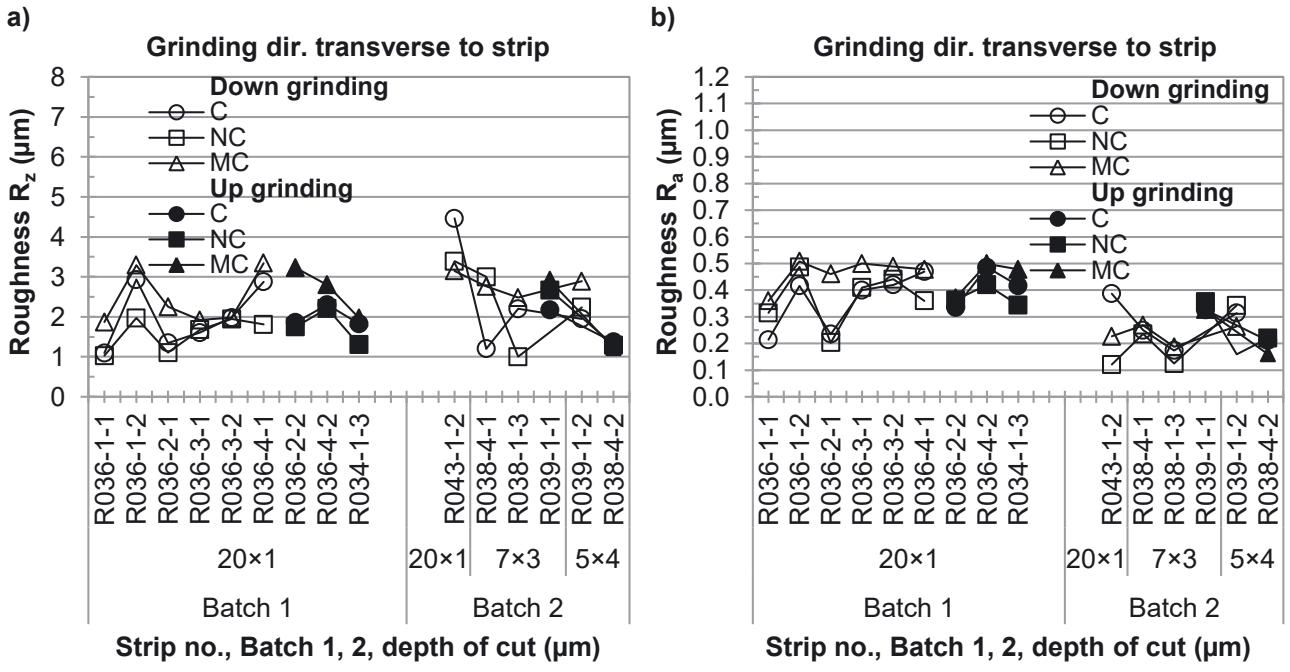

Figure 6: a) Roughness depths R_z and b) arithmetic mean roughness values R_a transverse to grinding grooves, i.e. longitudinal to the strips by grinding with different depths of cut in down and up grinding on measuring lines C, NC and MC of Batch 1 and 2.

Batch 2. The less uniform electrochemical deposition of the rounds from Batch 2 can also be seen in the layer thicknesses, which vary from 1.8 to 3 mm, in contrast to 1.4 to 1.7 mm for Batch 1. Thus, for R039-4-2 and R039-4-3 (Figure 1) of Batch 2 the values of compressive residual stresses transverse to strips (Figure 2c), at points C with –236 MPa (R039-4-2) and –110 MPa (R039-4-3) as well as at points NC with –230 MPa (R039-4-2) and –190 MPa (R039-4-3), are lower (Figure 7, solid lines) than those in longitudinal direction (Figure 7, dashed lines), at points C with –310 MPa (R039-4-2) and –190 MPa (R039-4-3) as well as at points NC with –314 MPa (R039-4-2) and –265 MPa (R039-4-3). Exactly the opposite occurs with R043-2-1 and R043-3-1 from quadrants 2 and 3 of Batch 2, which exhibit higher compressive residual stress values transverse (Figure 7, solid line) to the strip than longitudinal (Figure 7, dashed line) to it. The position of the strip in the quadrant apparently also can be of great significance, since the specimen R039-4-3 (position 3, in the fourth quadrant, Figure 1) taken closer to the edge has lower compressive residual stress values than the specimen R039-4-2 (position 2, in the fourth quadrant) taken closer to the middle of the round (Figure 7). In contrast to Batch 2, more uniform residual stresses are measured on the electrochemically deposited layers of Batch 1 (Figure 7, left).

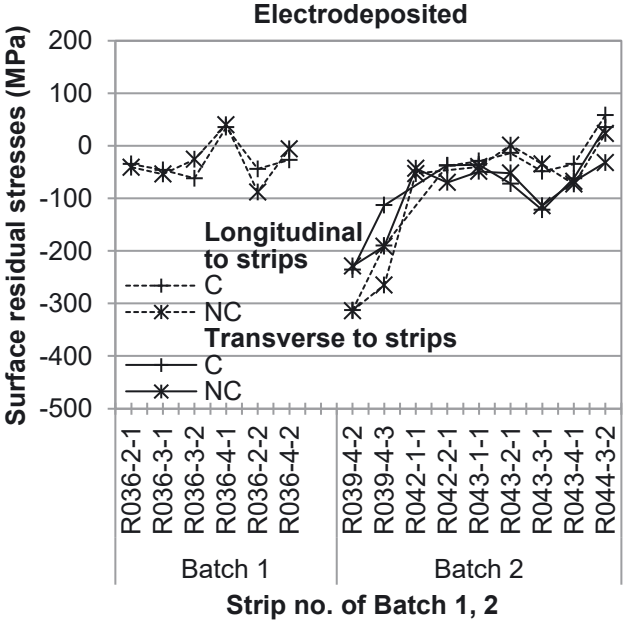

Figure 7: Surface residual stresses due to electrodeposition at measuring points C and NC longitudinal and transverse to strips of Batch 1 and 2.

For both finish down and up grinding with a small depth of cut 20 × 1 µm and likewise for electrochemical deposition, Figure 8 shows the surface residual stresses at points C, NC and MC of Batch 1. Transverse to the grinding direction, there is an increase in the compressive residual stress values compared to electrochemical deposition (Figure 8a, points C and NC). The residual stress states

differ significantly between down grinding (open symbols and solid lines) and up grinding (closed symbols and solid lines). When up grinding, the residual stress values clearly lie more in the compression range up to −500 MPa than after down grinding with up to −200 MPa. Furthermore, grinding provides approximately equal residual stresses at points C (open and closed circles) and NC (open and closed squares). This means that for the transverse ground strips there has to be a certain symmetry of the residual stress states with respect to the longitudinal axis of strips.

The surface residual stresses on the centerline of the strips at points MC for measurements longitudinal (open and closed triangles) and transverse (open and closed circles) to the grinding direction of the strips from Batch 1 depicts Figure 8b. In grinding or longitudinal direction (open and closed triangles), higher absolute residual stresses occur than in the transverse direction (open and closed circles). Small tensile residual stresses of up to 100 MPa are measured for down grinding (open triangles) and compressive residual stresses of −180 MPa (closed triangles) for up grinding. Transverse to the grinding direction, the measured residual stresses for down grinding (open circles) show values from about zero to −120 MPa, similar to those after electrochemical deposition (plus and stars). Up grinding (closed triangles and closed circles) again features absolutely lower residual stresses than down grinding (open triangles and open circles). About −350 MPa are achieved with up grinding. With regard to the position of the measuring points, there are certain differences in the residual stress values on the centerline at points MC versus the beginning and end of the respective grinding path at points C and NC (Figure 8).

The grain sizes measured in electrodeposited and in ground state, specifically on the surface at points C transverse to the grinding direction for the same strips of Batch 1 as in the residual stress analyses are shown in Figure 9a. After electrochemical deposition, the grain size at 9 nm is rather constant for all measured values (plus symbols), which corresponds well with previous results for the same current density of 3 A × dm^{-2} [33]. Grinding increases the measured grain sizes to about 13 nm. Here, the grain size values after down grinding are a little larger than after up grinding.

Micro strain change due to grinding compared to electrochemical deposition occurs in opposite manner than change in grain size (Figure 9b). The average micro strain at points C of the electrodeposited strips drops from 0.71 to 0.57% after down grinding and to 0.61% after up grinding.

The lattice constant of pure nickel of 0.3524 nm [64] increases to an average lattice spacing of 0.35326 nm for NiFe of Batch 1, electrodeposited (Figure 9c). When grinding the strips, the lattice spacing increases further to 0.354 nm for down grinding and to 0.35415 nm for up

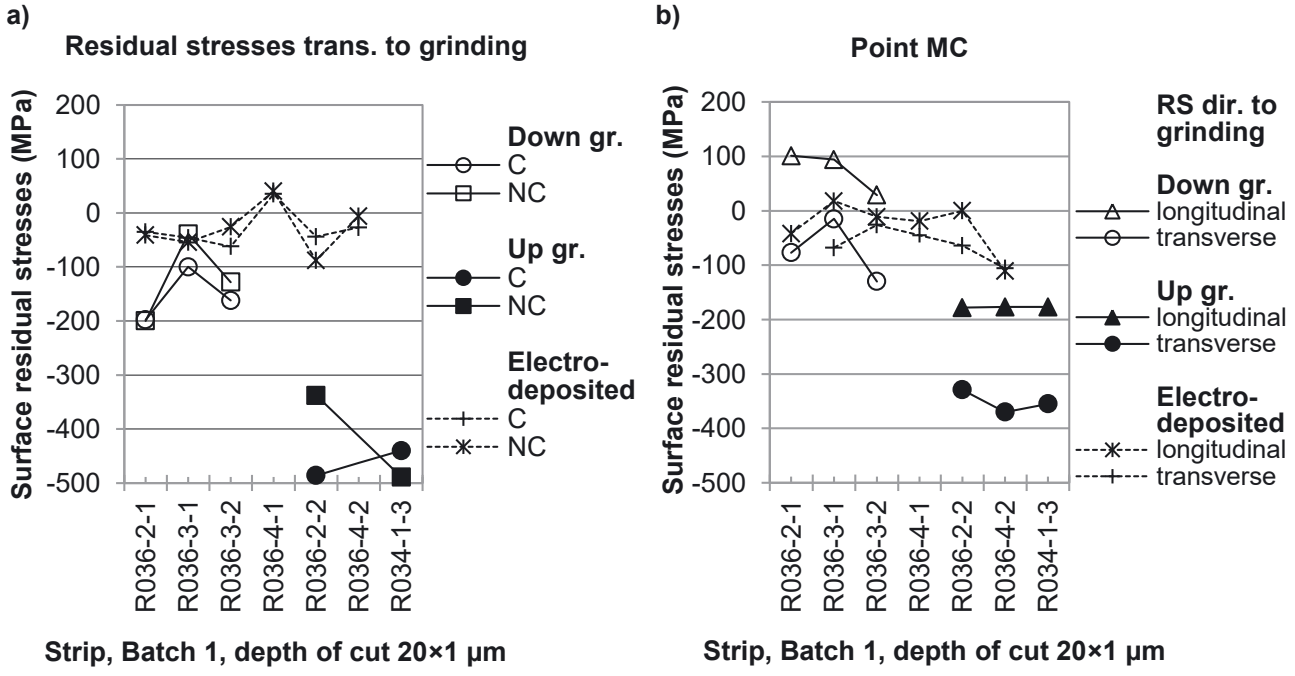

Figure 8: Surface residual stresses a) transverse to the grinding grooves at points C and NC and b) longitudinal and transverse to the grinding grooves at points MC by down and by up grinding with a depth of cut of 20 × 1 µm of strips of Batch 1.

grinding. Considered any state, the values are quite constant, with some exception of the up grinding.

The texture analyses are shown in Figure 10 at points C of the strips after electrochemical deposition and after grinding with 20 × 1 µm depth of cut. For these examples, the rotationally symmetrical pole figures of the {111}, {200} and the {220} lattice planes have a parallel position to the analyzed strip surfaces. Accordingly, the Harris texture index can be used for evaluation. Texture formation is evident by values greater than one for Harris texture index (Figure 10). All down and up ground strips with 20 × 1 µm depth of cut have {111} and {200} textures, as do the electrochemically deposited states.

Variations in depths of cut for Batch 2 strips result in the determined surface residual stresses in Figure 11. As the depth of cut increases slightly from 20 × 1 µm to 7 × 3 µm or

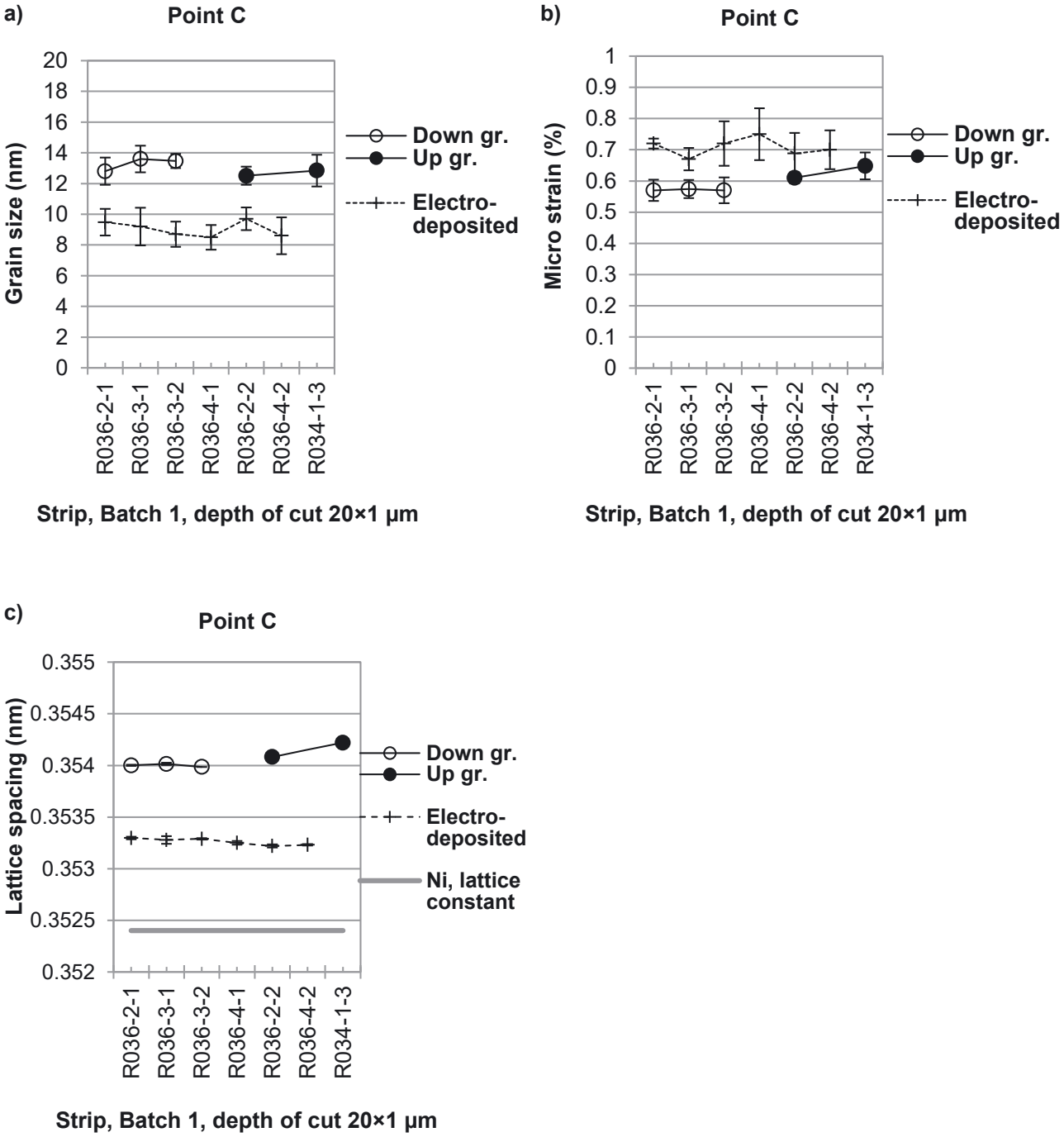

Figure 9: a) Grain size, b) micro strain, and c) lattice spacing, by down and up grinding with a depth of cut of 20 × 1 µm on the surface at points C of strips of Batch 1.

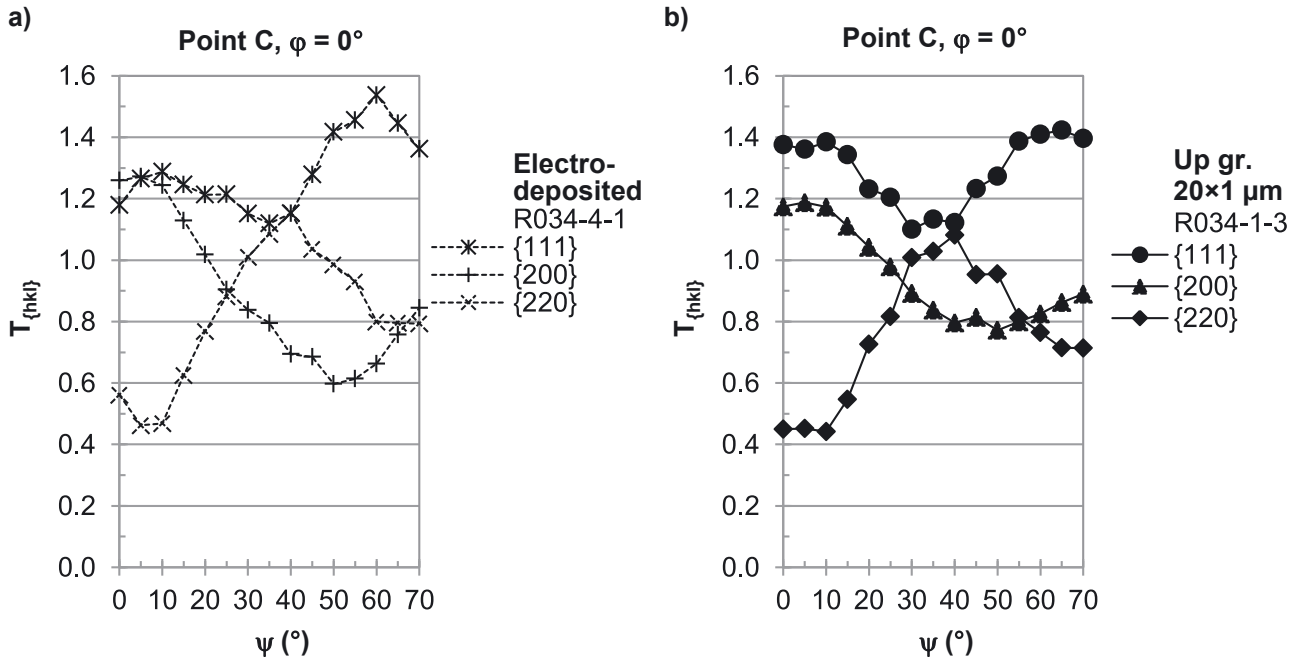

Figure 10: Harris texture index $T_{\{hkl\}}$ as a function of tilt angle ψ by a) electrodeposition of strip R034-4-1 and by b) up grinding with a depth of cut of 20 × 1 µm of strip R034-1-3 at points C of Batch 1.

5 × 4 µm, the residual stresses tend to increase. This is not the case with strip R039-1-2 for 5 × 4 µm depth of cut. Here the residual stresses decrease. Transverse to the grinding direction (Figure 11a), the residual stresses are absolutely smaller than longitudinal (Figure 11b) to it. On the grinding path, the residual stresses differ at points C and NC (Figure 2c) in particular for strip R038-1-3 (Figure 11a and b). The differences in the surface residual stresses after down grinding (open symbols) and after up grinding (closed symbols) do not show any unambiguous trends between the two grinding methods for the depths of cut 7 × 3 or 5 × 4 µm.

5 Discussion

The NiFe layer thicknesses of electrochemical deposition show a relatively narrow scatter range of 1.4 to 1.7 mm for Batch 1. Significantly larger scatter between 1.8 and 3.0 mm occurs in Batch 2. For grinding, each strip must be fixed to a specimen carrier with three screws (Figure 2) in a torque-optimized manner. As a result, the strips lie relatively flat and plane on the specimen carrier. With this preparation, rather uniform strip thicknesses are possible in grinding. In any case, careful defined grinding with a small depth of cut of 20 × 1 µm is required to achieve the best results.

Transverse grinding (Figures 3a and b) yield strip thicknesses with average values within the tolerance range of the desired nominal dimensions 320 ± 10 µm (Batch 1) and 330 ± 10 µm (Batch 2) of the respective strips. The smallest depth of cut of 20 × 1 µm resulted in mean values and standard deviations of 323 ± 2.1 µm after down grinding and 320 ± 0.9 µm after up grinding for Batch 1 strips (Figure 4, right and Figure 5, left), fitting very well within the target range of 320 µm. Also, the mean values for slightly increasing depths of cut from 20 × 1 to 7 × 3 or to 5 × 4 µm for Batch 2 strips of 332 µm for down grinding and 337.5 µm for up grinding (Figure 5, right) remain within the tolerance of 330 ± 10 µm. However, the standard deviations of most of these strips exceed the upper tolerance limit of 340 µm.

At the beginning of the investigations with parameters not always clearly defined, with longitudinally grinding (Figure 3c) of strips from the R032 round, Batch 1 (Table 1), the desired thickness could not be achieved (Figure 4, left). The mean value 340 µm with a rather large standard deviation ± 11.4 µm of the 12 strips lies clearly outside the target value 320 µm and the tolerance ±10 µm. The too large standard deviation may be related to the very thin strip thickness and the grinding path, which for R032 is three times as long (30 mm) as it would be possible in the width direction (10 mm), which means that the strips may be less rigidly fixed in the longitudinal than in the transverse

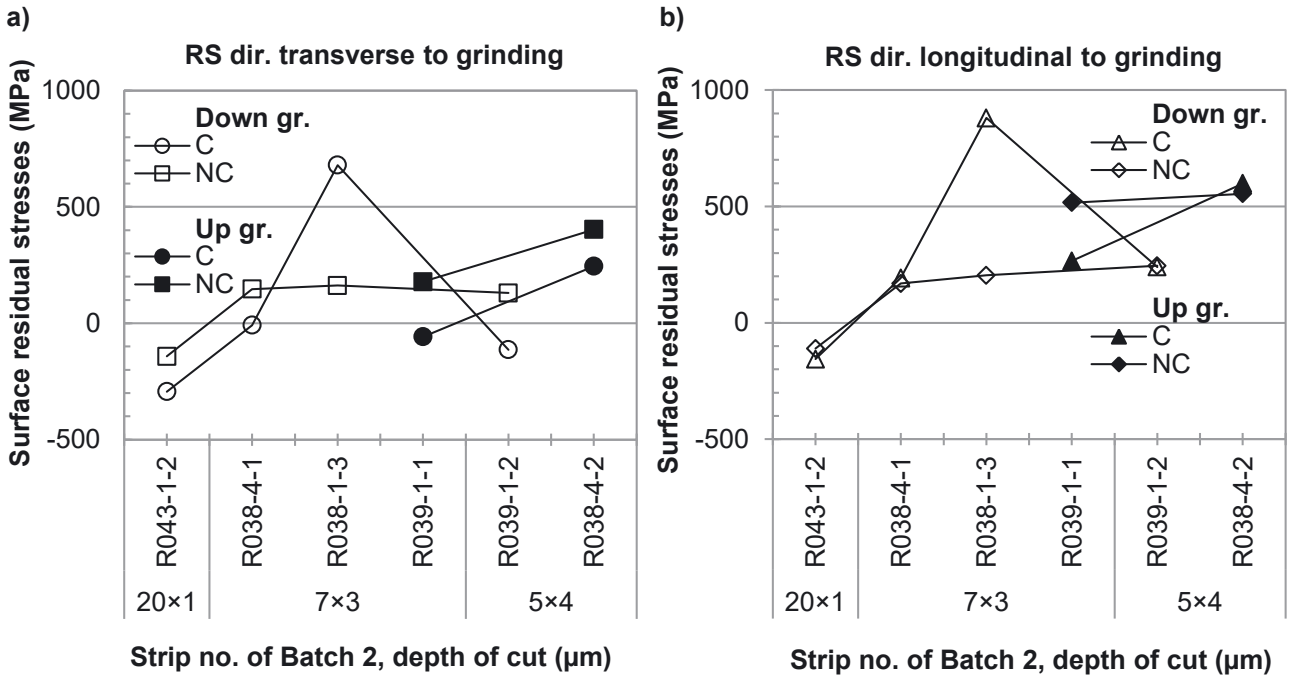

Figure 11: Surface residual stresses a) transverse and b) longitudinal to grinding for varied depths of cut by down and up grinding at points C and NC of strips of Batch 2.

direction. Weaker fixation of the strips in longitudinal than in transverse direction could be due to the different "free lengths" of the screw joints. It is a screw center distance of 12.5 mm in longitudinal and only 5 mm distance from the screw center to the strip edge in transverse direction (Figure 2b and c). Consequently, when grinding in the longitudinal direction, larger deformations of the strips and thus larger inaccuracies in the strip thicknesses could occur than in the transverse direction (Figure 4). Higher depths of cut of 7×3 or 5×4 µm (Figure 4, left and Figure 5, right) than 20×1 µm (Figure 4, right and Figure 5, left) also have a considerable influence. They cause higher scatter, especially in longitudinal but also in transverse grinding (Figures 4 and 5). In the case of the longitudinally ground samples, round R032 from Batch 1, another unfavorable influence on the greater scatter of the strip thicknesses could be the less defined dressing of the grinding wheel. Briefly, a defined grinding in the transverse direction with a small depth of cut of 20×1 µm produces the most accurate strip thicknesses.

Roughness values R_z of about 2.1 µm for the specimens of both Batches 1 and 2 hardly differ after finish grinding (Figure 6a). They are within the scatter range for varied depths of cut. Only the arithmetic mean value of the roughness R_a differs, as R_a has lower values for Batch 2 than for Batch 1 (Figure 6b). Here, the strips of Batch 2 are ground with largely identical parameters as Batch 1, with the exception of the slightly greater depth of cut in Batch 2. Compared to investigations on steel SAE 1045 or the superalloy GH4169, an increase and not a decrease in roughness would be expected with increasing depths of cut [17, 23]. But a comparison with these literature results is difficult because the literature takes into account both greater depths of cut during grinding and microcrystalline alloys.

The residual stress analyses by X-ray diffraction on the strip surfaces of nanocrystalline NiFe specimens must be performed under appropriate conditions. To find the most suitable measurement parameters, the results for different Bragg angles and increase the measurement time parameters were compared. For the Bragg angle, DIN EN 15305 recommends a reflection of more than $2\theta = 120°$. Comparative measurements are performed for the Bragg angles $2\theta^{\{420\}} = 155.675° > 120°$ of the {420} and for $2\theta^{\{311\}} = 92.933° < 120°$ of the {311} lattice planes [65]. However, for large Bragg angles, as for $2\theta^{\{420\}} = 155.675°$, less smooth interference lines with low intensity result even after very long measurement times. The most suitable interference lines arise for $2\theta^{\{311\}} = 92.933°$. Sufficiently high intensities and relatively smooth interference lines exist at this Bragg angle for all tilt angles up to $\psi = \pm 60°$. Line position distributions over $\sin^2\psi$ have good linearity for

both Bragg angles over the entire measurement range. This allows the well-known $\sin^2\psi$ method to be used for residual stress evaluation [57].

Figure 12 shows the measured surface residual stresses for the larger $2\theta^{\{420\}} = 155.675°$ and the smaller $2\theta^{\{311\}} = 92.933°$ Bragg angle at the same measuring points C for each case. It can be seen that the residual stress values for both Bragg angles mostly agree well. This is relevant for measurements transverse (Figure 12a) and longitudinal (Figure 12b) to the grinding direction. It is valid for all measured residual stress values from −500 to 900 MPa, according to the differently selected depths of cut for down grinding and for up grinding. An accuracy of this kind at the small Bragg angle $2\theta^{\{311\}} = 92.933°$ can be attributed in particular to the high setting accuracy of the goniometer. Here, the high manufacturing tolerances required and achieved in producing the diffractometer come in favor. All important setting positions of the goniometer have accuracies of ≤ 20 µm. Due to the more adequate interference lines, the residual stress measurements are carried out at $2\theta^{\{311\}} = 92.933°$. Owing to the linear lattice strain distributions over $\sin^2\psi$, no difficult evaluation of the lattice residual stress states of textured material is required.

X-ray diffraction is a widely used method for residual stress analysis and exhibits high resolution and usually high accuracy at microcrystalline metals [9, 11, 16, 22]. Moreover, residual stresses are very sensitive indicators of changes in the near-surface zones of the workpiece caused by variations in the grinding process [2, 5–7, 11, 12, 14–25]. In the case of the investigated nc NiFe alloy, this statement is confirmed for down and up grinding for different depths of cut, as shown by the X-ray measured surface residual stresses in Figures 8, 11, 12, 13, and 14.

Very careful finish grinding transverse to the strips with the smallest depth of cut of 20 × 1 µm results in low values of compressive residual stresses transverse to the grinding direction after down grinding and higher values of compressive residual stresses after up grinding for Batch 1 strips (Figures 8 and 13, left, and 14, left). According to an evaluation scheme, small depths of cut cause squeezing on the workpiece surface and are capable of generating compressive residual stresses. Thermal processes have no significant influence [2, 13–15]. The difference in residual stress formation between up and down grinding might be explained with the chip formation process similar to processes with defined cutting edges like milling. Applied to non-defined cutting edges in grinding, the following considerations arise. In up grinding, the wheel speed or cutting speed v_c and the table speed or workpiece speed v_w have opposite directions (Figure 3b). Material is removed from the thinnest to the slightly larger chip thickness (comma-shaped chips). So when the tool starts to engage on the newly formed surface, as in up grinding, squeezing

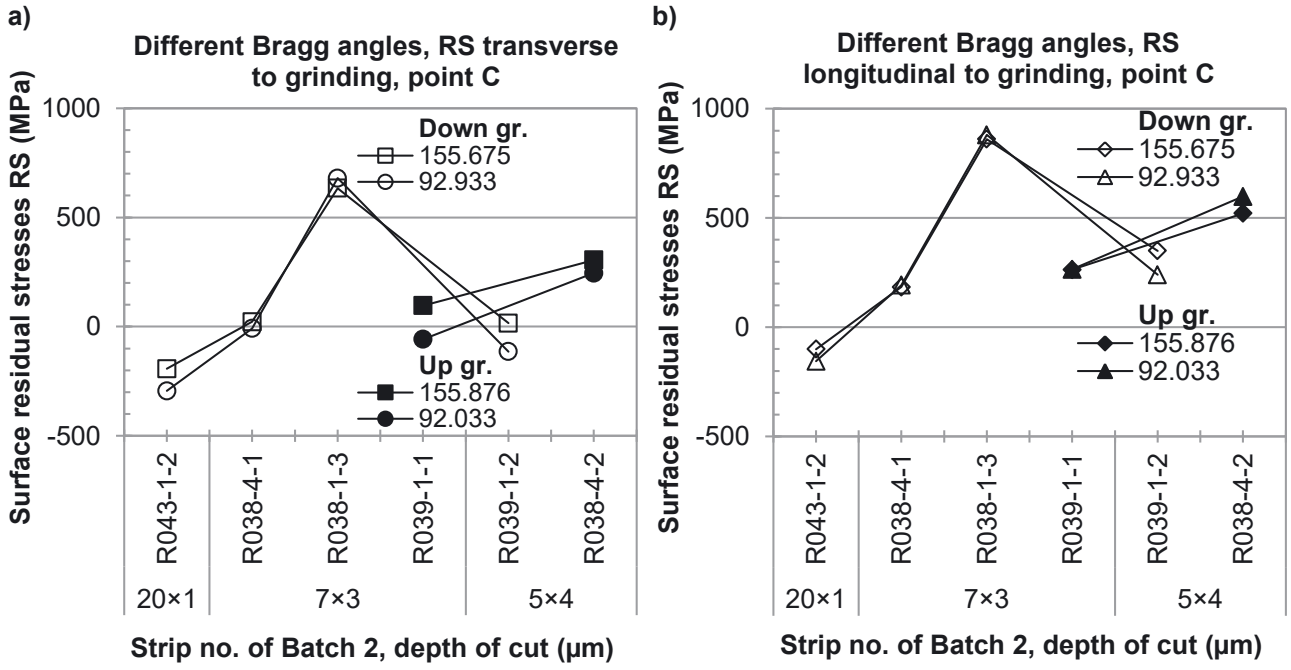

Figure 12: Surface residual stresses for different Bragg angles a) transverse and b) longitudinal to grinding for varied depths of cut by down and up grinding at points C of strips of Batch 2.

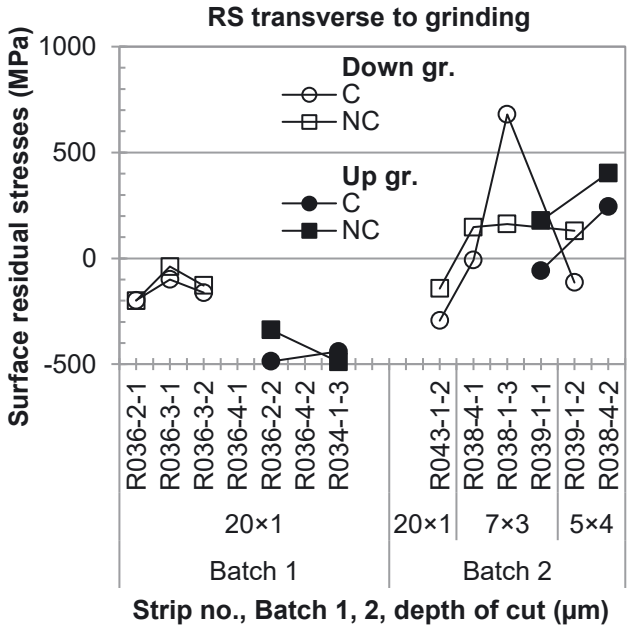

Figure 13: Surface residual stresses transverse to grinding by down and up grinding for varied depths of cut at points C and NC of strips of Batch 1 and 2.

processes and compressive residual stresses occur. In down grinding, the cutting speed v_c and the workpiece speed v_w have the same direction (Figure 3a) and the material is removed from the slightly thicker to the thinnest chip thickness, resulting in tensile residual stresses. The reason for this may be the longer contact time of tool and chip to the newly created workpiece surface during down grinding than during up grinding. Hence, the heat on the workpiece surface may be slightly higher. A further explanation is, that squeezing at the surface might be less in down grinding than in up grinding. Appropriate to the considerations, measurement results in creep feed grinding with low metal removal rates on 16MnCr5 indicate a higher temperature of the newly created surface for down grinding than for up grinding [19]. Heat on the newly created surface generates tensile residual stresses. Depending on the grinding parameters, e.g. low depths of cut dominate squeezing and thus compressive residual stresses and higher depths of cut dominate the heat generation and tensile residual stresses on the produced surface.

Increasing depths of cut can cause absolutely increasing surface residual stresses, as can be seen in Figures 11, 12, 13, and 14 for Batches 1 and 2. In down grinding, even a small increase in the depth of cut from 20 × 1 to 7 × 3 µm changes the sign of residual stresses from negative to positive values (Figures 11, 12, 13, and 14, open symbols). Highest tensile residual stresses result from down grinding for a depth of cut of 7 × 3 µm, in fact 880 MPa longitudinally and 680 MPa transversely to grinding direction for strip R038-1-3 from Batch 2 at measuring point C (open triangle and open circle in Figures 11, 12, 13, and 14). Up grinding with increasing depths of cut from 20 × 1 to 7 × 3 or to 5 × 4 µm also increases the surface residual stresses from negative to positive values (closed symbols, Figures 11, 12, 13, and 14). In turn, in the longitudinal grinding direction the highest values arise, for a depth of cut of 7 × 3 µm 265 MPa at point C and 516 MPa at point NC for strip R039-1-1 (Figure 11b, closed triangle and closed diamond). The maximum for up grinding with a depth of cut of 5 × 4 µm results in 598 MPa at point C and 554 MPa at point NC for strip R038-4-2 (Figure 11b, see closed triangle and closed diamond). In the measured transverse direction for a depth of cut of 7 × 3 µm, the lower values reach –58 MPa, point C and 178 MPa, point NC, strip R039-1-1 (Figure 11a, closed circle and closed square). The maximum in the transverse direction for up grinding with a depth of cut of 5 × 4 µm results in 245 MPa at point C and 403 MPa at point NC for strip R038-4-2 (Figure 11a, see closed circle and closed square).

Large scatter especially after down grinding with the higher depths of cut of 7 × 3 or 5 × 4 µm (see open symbols in Figures 11, 13, and 14), Batch 2, must be taken into account when assessing the residual stresses. Identical depth

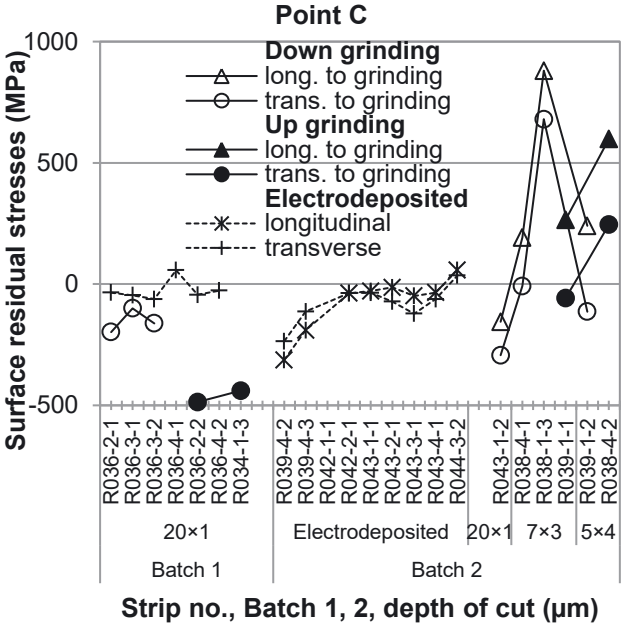

Figure 14: Longitudinal and transverse surface residual stresses of electrochemically deposited strips as well as of strips ground transverse in down and up grinding with varied depths of cut at points C of Batch 1 and 2.

of cut of 7 × 3 µm thus results in transverse residual stresses of −8 and 147 MPa for strip R038-4-1 at points C and NC (open circle and open square) and 680 MPa at point C (open circle) and 130 MPa at point NC (open square) for strip R038-1-3 as shown in Figures 11a and 13. Likewise, the longitudinal residual stresses of 880 and 204 MPa of strip R038-1-3 at point C (open triangle) and point NC (open diamond) differ significantly with the same grinding parameters to strip R038-4-1 with 192 MPa at point C (open triangle) and 169 MPa at point NC (open diamond), as can be seen in Figure 11b. In addition, the residual stresses at the slightly higher depths of cut from 7 × 3 to 5 × 4 µm for strips R038-1-3 to R039-1-2 even drop significantly instead of increasing (see open symbols, Figures 11, 12, 13, and 14). Thus, in the transverse measuring direction the values change from 680 MPa to −114 MPa, points C, and from 162 to 130 MPa, points NC (see open circles and squares, Figure 11a), and in the longitudinal direction from 880 to 240 MPa, points C, and increase slightly from 204 to 245 MPa, points NC (see open triangles and diamonds Figure 11b). As an explanation, it is known from microcrystalline metals that the original residual stresses before grinding have a significant influence on the resulting residual stresses after grinding [16]. Then, in the case of nc NiFe, the residual stresses after electrochemical deposition, i.e. before grinding, may affect the very different residual stresses after grinding. Especially round R039 shows the largest deviations in the compressive residual stresses after deposition (Figures 7 and 14, plus and star signs). During electrochemical deposition, several factors can influence residual stress formation [41–50]. This includes differences in the composition of the industrial baths, which cannot be ruled out for the rounds examined, as they were deposited at different times. Accordingly, the layer thicknesses after deposition show large differences of 1.8–3 mm, especially for the layer strips from Batch 2.

Less uniform grinding at higher depths of cut may be another reason for the very different residual stresses between strips R038-4-1, R038-1-3 and R039-1-2, especially in down grinding. Already the strip thicknesses after finish grinding show less uniform results with higher standard deviations at higher depths of cut of 7 × 3 or 5 × 4 µm than at 20 × 1 µm (Figures 4 and 5). Larger scattering of the locally measured strip thicknesses indicates that the adjusted depths of cut and the actual locally acting depths of cut may not match. Locally different depths of cut probably result from larger deformations during finish grinding of the very thin strips with larger depths of cut. Even small deformation differences in the µm range and thus small differences in the actual local depth of cut are probably sufficient to produce correspondingly large differences in the local residual stresses. Maximum differences can be seen in strip R038-1-3 between points C and NC for both transverse and longitudinal residual stresses (Figure 11a and b and Figure 13, open symbols, circles and squares, and triangle and diamond). All this is possible, because the very thin strips can be deformed more easily during finish grinding due to the higher depths of cut with higher grinding forces.

The measured effect of increasing surface residual stresses with increasing depths of cut for nc NiFe is similar to that for conventional microcrystalline metals [2, 5–7, 14–17, 20–24]. Depending on whether the influence of cold plastic deformation or that of rapid heating-cooling cycle with thermal plastic deformation predominates, residual stress states close to the surface occur with a negative (compressive residual stresses) or positive (tensile residual stresses) sign. Basically, both influences overlap, with the heat influence increasing as the depth of cut increases. Further increasing depths of cut can cause higher temperatures and microstructural transformations that additionally influence the residual stress state. Sometimes, in extreme cases, cracks can also occur. However, such problems do not exist in the investigations carried out, since the distance between the measured maximum tensile residual stress 880 MPa and the yield strength 1700 MPa of the electrodeposited material appears large [32, 33]. The transition from surface compressive stress to surface tensile stress with increasing depths of cut cannot be determined exactly due to the scattering. Even with the very narrow variation of the depth of cut from 20 × 1 to 7 × 3 or to 5 × 4 µm, stronger scattering of the residual stresses occurs (Figure 11). This is comparable to microcrystalline metals, where the transition from surface compressive stresses to surface tensile stresses with increasing depths of cut also does not exhibit absolutely exact values. Furthermore, such behavior depends on the workpiece material itself and on the overall grinding parameters chosen. When grinding SAE 1045 (C45E) steel, for example, with ceramic wheels and emulsion as coolant, the sign changes from negative to positive residual stress values in the quenched and tempered state for depths of cut between 4 and 11 µm and in the hardened condition between 4 and 15 µm [2, 5–7, 14, 15]. Another study reports on the grinding of hardened SAE 1045 steel [17]. SiC grinding wheels produce compressive residual stresses with depths of cut of 10 µm and tensile residual stresses with 40 µm. If CBN grinding wheels are used, the surface residual stresses remain in the compressive range even after 70 µm. Grinding of hardened steels of higher carbon content with a ceramic grinding wheel and coolant results in the transition between negative and positive surface residual stresses for depths of cut

from 3 to 11 µm [20]. Using a CBN grinding wheel shifts the generation of tensile residual stresses to much higher depths of cut. A nickel superalloy GH4169 shows surface tensile residual stresses when using a ceramic grinding wheel with emulsion, which increase in the range of the selected depths of cut from 5 to 40 µm [23]. Results on another nickel superalloy K417 reveal the same direction of change in residual stresses, but without detailed information on the depths of cut [24]. It is worth pointing out also that the literature often additionally varies other parameters such as cutting speed or workpiece speed. Grinding power has a similar influence as the depth of cut. Increasing the specific grinding power leads to increasing residual stresses in conventional mc metals, likewise with a scatter range [11, 12]. No such studies are known for nanocrystalline metals.

Up grinding produces absolutely smaller residual stresses than down grinding, which is known from milling of mc metals [2, 5, 9, 14, 15]. In the results presented, this is the case for grinding nc NiFe with small depths of cut of 20×1 µm (Figure 8). A larger depth of cut of 7×3 µm also produces absolutely smaller residual stresses of −58 MPa, strip R039-1-1 (closed circle) transverse to the grinding (Figure 11a) at points C during up grinding than during down grinding with −8 and 680 MPa, strip R038-4-1 and R038-1-3 (open circles). Looking at the corresponding measurement results in the NC points, the residual stress values are approximately the same for both grinding methods, for up grinding 178 MPa, R039-1-1 (closed square) and for down grinding 147 and 162 MPa, R038-4-1 and R038-1-3 (open squares). Comparing the measuring points C and NC in Figure 11a, for down grinding only −8 MPa of strip R038-4-1 (point C, open circle) is significantly smaller than for up grinding 178 MPa of strip R039-1-1 (point NC, closed square). In the longitudinal direction in Figure 11b, however, up grinding with a depth of cut of 7×3 µm at the NC measuring points results in a significantly higher residual stress value of 516 MPa (closed diamond) for strip R039-1-1 than down grinding with 169 and 204 MPa (open diamonds) for strips R038-4-1 and R038-1-3. At measuring points C, the residual stress values for both grinding methods are about the same in up grinding with 265 MPa (R039-1-1, closed triangle) and in down grinding with 192 MPa (R038-4-1, open triangle), or even significantly higher in down grinding with 880 MPa (R038-1-3, open triangle). In addition, the residual stress values for depths of cut of 5×4 µm for up grinding are larger at 598 and 554 MPa (C, closed triangle and NC, closed diamond) for strip R038-4-2 than for down grinding at 240 and 245 MPa (C, open triangle and NC, open diamond) for strip R039-1-2 (Figure 11b). The absolute smaller values of strip R039-1-2 after down grinding in both longitudinal and transverse direction (Figure 11), are related to the relatively large compressive residual stresses of round R039 after electrochemical deposition (Figure 7). But the relatively high residual stress value of 516 MPa of strip R039-1-1, which is also present in round R039, does not really match this consideration (Figure 11b, closed diamond). Nevertheless, down grinding with a depth of cut of 7×3 µm even leads to the highest measured tensile residual stresses with 680 MPa (open circle) in the transverse direction and 880 MPa (open triangle) in the longitudinal direction at point C of strip R038-1-3 (Figure 11).

Corresponding microstructure investigations in the near-surface area were examined for measuring points C. Based on rotationally symmetrical pole figures before and after grinding, it is assumed that the microstructures in the measuring plane do not depend on the direction. So, the grain sizes of the electrochemically deposited strips from Batch 2 in both directions, transverse and longitudinal, agree well in single and also with the respective mean values 9.4 and 9.6 nm (Figure 15a, plus and star signs). The measured {111} and {200} textures have their lattice planes parallel to the strip planes. This applies to electrochemical deposition as well as to the down/up grinding. Figure 10 confirms similar texture characteristics for electrochemical deposition as for grinding with depths of cut of 20×1 µm, using the Harris texture index.

Slightly increasing grain sizes are observed both after grinding with small 20×1 µm (Figure 9a, Batch 1) and with larger depths of cut of 7×3 or 5×4 µm (Figure 15a, Batch 1 and 2). Looking at the grain size for a small depth of cut of 20×1 µm (Figure 9a, Batch 1), there tends to be few larger single values after down grinding (open circles) than after up grinding (closed circles). Accordingly, average values at 13.3 nm in down grinding and 12.7 nm in up grinding obtained, starting from 9.0 nm (plus sign) after electrochemical deposition.

Down grinding with a small depth of cut of 20×1 µm of the strip R043-1-2, Batch 2, results in a grain size of 15.9 nm (Figure 15a, right, open circle). This value ranges slightly higher than the comparable three single values of the strips from Batch 1 or their mean value 13.3 nm (Figures 9a and 15a, left, open circles). Enhanced depth of cut of 7×3 µm causes grain sizes to increase to 19.2 (R038-4-1, open circle) and 23.4 nm (R038-1-3, open circle). However, for the depth of cut of 5×4 µm, there is a significant drop in grain size to 13.1 nm for strip R039-1-2 (Figure 15a, right, open circle). Analogously to the development of the residual stresses (Figure 14, open circles and also open triangles) of ground strips, it can also be observed for the grain sizes (Figure 15a,

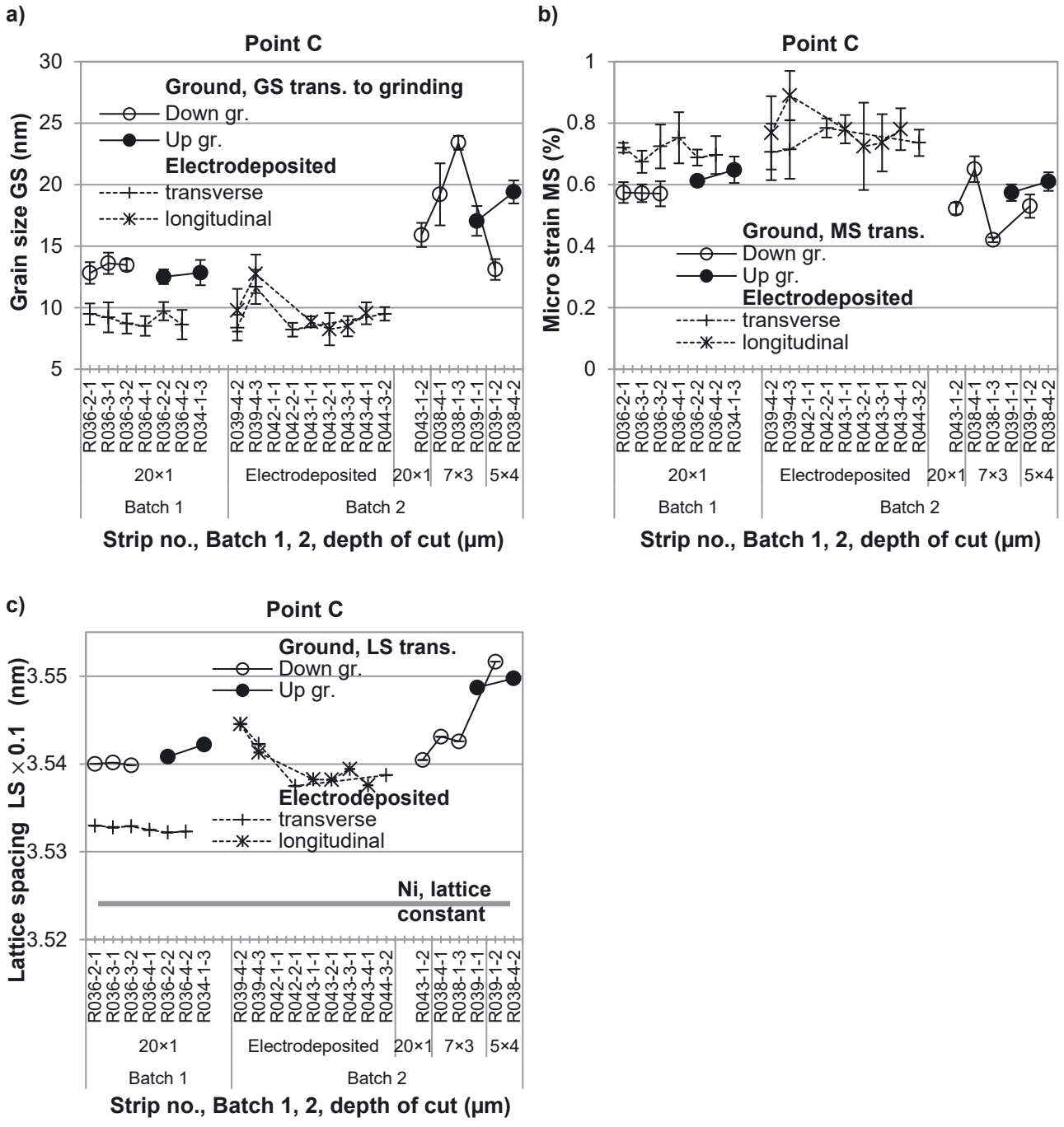

Figure 15: a) Grain size, b) micro strain and c) lattice spacing on the surface of electrochemically deposited strips as well as of strips ground transverse in down and up grinding with different depths of cut at points C of Batch 1 and 2.

right, open circles), that first an increase and then a decrease of the measured values occurs with an increase of the depth of cut.

Up grinding with depths of cut of 7 × 3 and 5 × 4 µm also causes an increase in the measured grain sizes to 17.0 and 19.4 nm, strips R039-1-1 and R038-4-2, Batch 2 (Figure 15a, right, closed circles). As depicted in Figure 15a, these are above those of electrochemical deposition (plus and star signs) and are more or less larger than after up grinding (closed circles) and down grinding (open circles) of Batch 1 as well as in down grinding of Batch 2 (open circle, R043-1-2) with small depth of cut of 20 × 1 µm. Moreover, up grinding leads to a small increase in grain sizes with increasing depths of cut when looking at both batches.

The comparison of micro strains for the electrodeposited layer strips shows slightly lower values for Batch

1 (plus sign) than for Batch 2 (plus and star signs), on average 0.71%, Batch 1 and 0.74%, Batch 2 (Figure 15b). Batch 2, measured transversely and also longitudinally, once again has a greater scatter. However, the measured values in these two directions can hardly be distinguished, as they mostly appear within the scatter range. The grinding process (open and closed circles) reduces micro strains compared to the initial state of electrodeposition, as depicted in Figures 9 and 15b. Down grinding (open circles) usually results in somewhat larger decreases in micro strains than up grinding (closed circles). At a small depth of cut of 20 × 1 µm, Batch 1, the average values are 0.57% for down grinding and 0.61% for up grinding. Applying the same low depth of cut of 20 × 1 µm in down grinding for strip R043-1-2 from Batch 2 results in an even smaller value 0.52% (Figure 15b, right, open circle). Increased depths of cut of 7 × 3 and 5 × 4 µm cause approximately the same or more decreasing micro strains than 20 × 1 µm. Strip R038-1-3 with the highest tensile residual stresses features the smallest micro strain of 0.42%.

Based on the lattice constant of pure nickel, the lattice spacing increases with electrochemically deposited NiFe (Figure 15c). Fairly constant lattice spacings again illustrate the much more uniform states for Batch 1 (plus signs) than for Batch 2 (plus and star signs). In addition, the values for Batch 2 are higher than for Batch 1. It is known from the literature that the lattice spacing of NiFe increases linearly up to about 50 wt% of iron [32, 38, 41]. Therefore, Batch 2 must be assumed to have a higher and more irregular iron content than Batch 1. Grinding (open and closed circles) further increases the lattice spacing of the strips from Batch 1 and apparently also from Batch 2. Here, however, it should be noted that a comparison only provides unambiguous results for the same specimens in each case. The analyses at Batch 1 are carried out on the same specimens, first after electrochemical deposition and then after grinding. This was not the case with the specimens of Batch 2. However, the specimens from rounds R039 and R043 also yield larger lattice spacings after grinding than after electrochemical deposition (Figure 15c). Furthermore, the measured values after up grinding are larger or about the same as after down grinding. In this context, the residual stresses must also be taken into account, often having absolutely smaller values after up grinding than after down grinding. An explanation for this is that compressive residual stresses might increase and tensile residual stresses might decrease the determined lattice spacing (compare Figures 14 and 15c). With respect to the measured texture, the considered lattice spacing <100> is orientated perpendicular to the specimen surface and is stretched for surface-parallel compressive residual stresses and compressed for tensile residual stresses.

Various comparisons of surface states can be considered in Figure 16. In this way, Figure 16a compares the surface residual stresses with the associated grain sizes. The reference state is provided by the electrochemical deposition data with the smallest grains and with low residual stress values as a circled cluster of plus and star signs on the left of the figure (Batches 1 and 2). However, some data from layer strips of Batch 2 (brighter plus and star signs) localize somewhat outside the circled area at larger compressive residual stress values or grain sizes.

The grinding residual stresses versus the grain sizes as a rising scatter band can be seen in Figure 16a. Due to the scattering, it is difficult to make a comparative statement between down grinding (open symbols) and up grinding (closed symbols). Therefore, corresponding regression lines are plotted in Figure 16a. In the case of down grinding, measured in the longitudinal direction, it is the upper dashed regression line. For up grinding, also measured along the grinding direction, the solid connecting line of two measuring points (closed triangles) even runs at the very top. Residual stresses measured longitudinally to the grinding direction thus arrange themselves above the other results (open and closed triangles). Measured in the transverse direction, the lower dashed regression line and the lower solid regression line agree well for down and up grinding. In any case, the residual stresses clearly rise with the grain sizes. A reason for this behavior could be attributed to increasing heat generation during the grinding process. As it is known from the literature, grinding with larger cutting depths generates more heat than with smaller cutting depths [2, 14–17, 20, 23, 24]. But Figure 16 intentionally does not give any information about the depth of cut. This is because for small strip thicknesses as 320 or 330 µm, there may be differences between the depths of cut set on the machine and the locally acting cutting depths due to strip deformation during grinding. This same explanation might also be used to understand the strong scattering of the residual stresses in Figures 11, 12, 13, and 14 in down grinding for the set depths of cut of 7 × 3 or 5 × 4 µm. Since the residual stress and microstructure analyses are each carried out at the same point on the strips, the surface states in Figure 16 should fit each other regardless of the set depths of cut. The decisive factor should therefore be the locally effective depths of cut for these thin strips. They remain unknown, but should generate more heat at higher values.

The grain size increase during grinding, even at a small depth of cut of 20 × 1 µm, is most likely due to the extremely

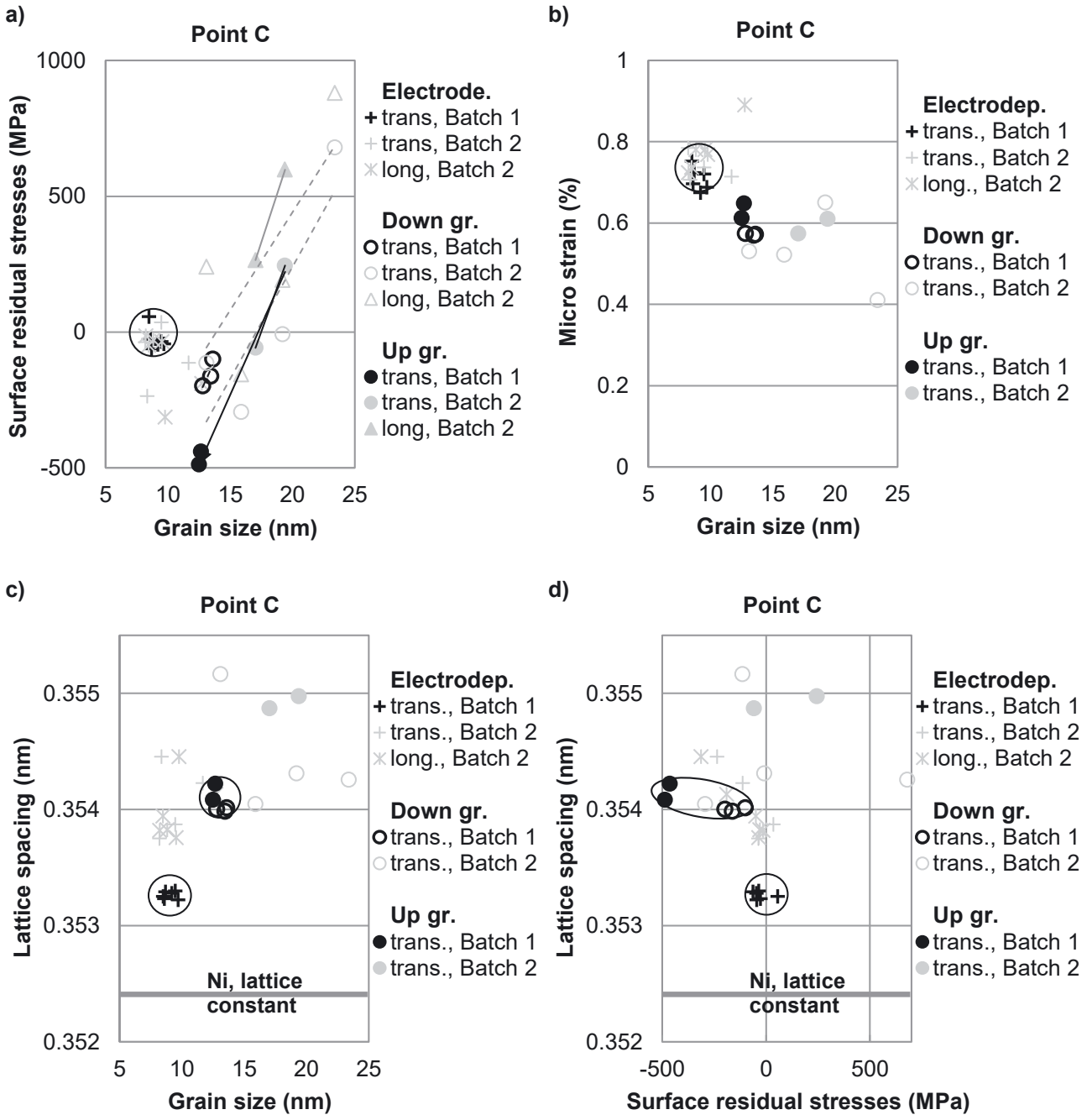

Figure 16: a) Surface residual stresses, b) micro strains and c) lattice spacings versus grain sizes as well as d) lattice spacings versus surface residual stresses for electrochemically deposited and for differently ground strips at points C of Batch 1 (surrounded with a circle as well as with ellipse) and Batch 2.

small grain sizes with the high grain boundary volume and the resulting significantly lower thermal stability of nanocrystalline than of conventional microcrystalline metals [26, 66–68]. For example, for pure nc nickel without additives with a grain size of 10 to 20 nm, nucleation and abnormal grain growth have been determined by differential thermal analysis (DTA) and correspondingly by transmission electron microscopy (TEM) at 80 °C and 120 °C, respectively [66]. Abnormal/bimodal grain growth represents the incipient primary recrystallization and signifies the growth of a few grains in the surrounding nanocrystalline microstructure. Nickel-iron alloys exhibit improved thermal stability and higher grain growth temperatures than pure nickel [26, 68]. With increasing iron

content from about 6 wt% to 18 wt%, the temperatures for that grain growth begin to shift slightly to higher values from 220 to 260 °C. A final primary recrystallization takes place with an annealing at 300 °C. Grain growth also depends on the duration of the annealing process, which in the literature turns out to be significantly longer than the relatively fast heating-cooling cycles of grinding. Nevertheless, the high grain boundary energy of the extremely small grains and the high grain boundary volume, which accounts for about 50 to 25% at grain sizes of 5 to 10 nm [66, 69], must cause grain growth already at fairly low temperatures and, before that, a reduction of micro strains at even slightly lower temperatures.

Micro strains will be relieved in annealing treatments of electrodeposited nickel or nickel-iron alloys at very low temperatures [67, 68, 70–72]. At these temperatures, recovery processes begin and no grain growth or change in grain structure takes place yet. Heating of nc nickel specimens of grain size 10 nm by differential scanning calorimetry (DSC) analyses at a rate of 10 °C × min^{-1} leads to stress relaxation already at approx. 60 °C [72]. Nickel deposited with additives (saccharin) reduces its micro strains annealed at 100 °C/1 h from 0.313 to 0.211% [70]. Alloying or impurity atoms such as sulfur from additives, or second phases can improve the thermal stability during the heat treatment by deposition processes at the grain boundaries. So, for Ni-21 wt% Fe, a small decrease in micro strains from 0.29 to 0.27% is observed after annealing at 100 °C/1 h [67]. Own investigations on similar electrodeposited nickel-iron alloys as in the present investigations with 6 to 18 wt% Fe show the onset of recovery at 200 to 240 °C/2 h shortly before the onset of recrystallization at 220 to 260 °C/2 h [32, 68]. Depending on the iron content, the micro strains in this case range from 0.35 to 0.7% before annealing. The recovery process is finished at temperatures of 280 to 300 °C/2 h with micro strains of 0.02 to 0.1% and the process of primary recrystallization at 300 °C/2 h.

With the selected grinding parameters and the associated short heating and cooling cycles, it seems to be possible to decrease the micro strains and at the same time slightly increase the values of the grain size, starting from electrochemical deposition (Figure 16b). To achieve this, it assumes that grinding generates sufficient heat. As Figure 16b reveals, greater depths of cut of 7 × 3 or 5 × 4 µm in strips of Batch 2 (brighter pluses and stars to brighter open and closed circles) cause a stronger decrease in micro strains than a smaller depth of cut of 20 × 1 µm in Batch 1 (darker pluses to darker open and closed circles). Maximum reduction of a micro strain to 0.41% (bright open circle, bottom right of Figure 16b) and the more pronounced increase in grain size to 23.4 nm occur for strip R038-1-3 with the highest tensile residual stresses 680 MPa (transverse) and 880 MPa (longitudinal) measured after down grinding with a depth of cut of 7 × 3 µm (Figure 14). Furthermore, a greater decrease in micro strain tends to be observed when down grinding (open circles) than when up grinding (closed circles). Cause for a stronger decrease in micro strain can be a higher heat development on the workpiece surface when grinding with greater depths of cut and when down grinding.

Lattice spacings, shown in Figures 15c and 16c, increase during grinding (open and closed circles), starting from electrochemical deposition (plus and star signs). Results of Batch 1 specimens, surrounded by a circle, show a smaller scatter than Batch 2 specimens (Figure 16c). The values of Batch 2 specimens after electrochemical deposition as well as mostly after grinding are higher than those of Batch 1 (brighter to darker plus and stars as well as brighter to darker open and closed circles). Up grinding (closed circles) usually yields slightly larger values for the lattice spacing than down grinding (open circles).

Lattice spacings and surface residual stresses plotted against each other can be seen in Figure 16d. There is a tendency toward decreasing lattice spacing with increasing grinding residual stresses for Batch 1 (closed and open dark circles, surrounded by an ellipse) and also for Batch 2 (bright, closed and open circles). I.e. compressive residual stresses increase and tensile residual stresses decrease the lattice spacing. However, the increase in lattice spacing due to grinding cannot be explained by the measured surface residual stresses alone, as the lattice spacing does not change very much with the residual stresses. Similarly, for electrochemical deposition, a decreasing trend of lattice spacing with increasing residual stresses (plus and star signs) is evident.

An increase in the lattice spacing with a simultaneous decrease in micro strain during grinding cannot be easily understood (Figures 16b and c), because an increasing lattice spacing would have to be associated with increasing lattice defects in the nanocrystals and thus increasing micro strain. Annealed nc NiFe alloys in turn show decreasing micro strain due to decreasing dislocation densities and dislocation sources at the grain boundaries as well as a redistribution of finest atomic impurities from the grain interior to the grain boundaries (e.g. sulfur from saccharin) [67, 68, 70, 71]. Low annealing temperatures, about 200 °C to 250 °C depending on the iron content, thus lead to a reduction of the micro strain due to modifications of the grain boundaries, with incipient grain growth, without dislocations within the grains and with few at the grain boundaries. Very short heating-cooling cycles during

grinding, though, can make it difficult for alloy or impurity atoms to diffuse. Nevertheless, local grain growth occurs in nc crystals due to the high grain boundary energy and the high grain boundary mobility. The resulting anomalous microstructure grows with individual larger grains into the surrounding nc matrix. In the process, the original grain boundaries with their high volume fractions of 50 to 25% at the growth front dissolve into the new larger crystals with negligible grain boundary volumes. Vacancies, alloying and impurity atoms from the original nc microstructure and from its grain boundaries must be incorporated into the recrystallizing grains without significant diffusion. Higher alloy or impurity atom concentrations inside the recrystallized crystals and lower dislocation densities at the grain boundaries could thus explain the increase in the measured lattice spacing together with the decreasing micro strain.

When considering the X-ray surface analyses, it must be taken into account that the primary beam diameter 200 µm irradiates many grains of the anomalous/bimodal microstructure. Recrystallized grains and the surrounding nc matrix are detected together. I.e. decreasing grain boundary volumes and with it decreases in volume in the area of the recrystallized larger grains can have an effect on the X-ray residual stress analyses. Hence, the local volume reductions of the recrystallized grains would cause a material shrinkage in the near-surface zone. In doing so, the surface residual stresses of type I shift to absolutely higher values. Type II tensile residual stresses additionally form in the area of the recrystallized grains. The measured residual stresses thus represent superpositions of the residual stresses of type I and type II. Furthermore, the determined grain sizes must be considered as mean values from the grown recrystallized grains and the surrounding nc matrix. In order to detect the nanocrystalline and recrystallized grain size distributions separately, TEM investigations would be necessary [71].

6 Conclusions

Thin strips of electrochemically deposited nanocrystalline nickel-iron are produced with a surface grinding machine. Grinding of defined surface states, especially with the desired thin strip thicknesses of 320 or 330 µm, really is a demanding challenge in this case. A necessary requirement for grinding involves carefully mounting the thin strips on a specimen carrier. By varying the depths of cut and the type of grinding method, down or up grinding, different surface states can be achieved. An X-ray diffractometer with a primary beam diameter of 200 µm serves to measure the residual stresses and near-surface microstructural states. It means that the results derive from the total irradiated surface in each case. Hence, the determined grain sizes after grinding represent mean values from a few recrystallized new larger grains and from the surrounding original, finer nanocrystalline matrix.

In the electrochemically deposited initial state before grinding, the specimens from Batch 1 have a much more uniform quality than those from Batch 2. It applies both to the thicknesses of the deposition layers and to the measured surface residual stresses, which for Batch 1 mostly have low values in the compression range. Only one specimen exhibits low tensile residual stresses after electrochemical deposition. Batch 2 scatters significantly more in these and also in the microstructure values. Irrespective of this, the mean values of the near-surface microstructural states after electrochemical deposition differ only slightly between Batches 1 and 2. Averaged over several specimens, grain sizes of 9 nm (Batch 1) as well as 9.5 nm (Batch 2) and micro strains of 0.71% (transverse, Batch 1) as well as 0.74 and 0.78% (transverse and longitudinal, Batch 2) are obtained.

When grinding in the transverse direction, the smallest depths of cut of 20 × 1 µm give the best results (Batch 1). All measured values of the strip thicknesses come within the tolerance range. Likewise, rather uniform values are achieved for the measured microstructural states. In contrast, there exist considerable differences in the surface residual stresses. After up grinding, the absolutely lowest compressive residual stresses occur transverse to grinding direction, up to –500 MPa. For down grinding, the absolute lowest values occur at –200 MPa for Batch 1 strips and –300 MPa for Batch 2 strips. Longitudinally to the grinding direction, the values obtained tend to be about 100 to 300 MPa higher than transversely to it. Surface roughness of the two grinding methods in turn shows no significant differences. Both types of grinding methods and all selected depths of cut 20 × 1 or 7 × 3 or 5 × 4 µm (Batches 1 and 2) result in similar roughness values R_z of about 2.1 µm. Only the R_a values remain slightly lower at the higher depths of cut.

A larger depth of cut of 7 × 3 µm in down grinding produces the highest surface residual stresses of 880 MPa in the grinding direction and 680 MPa in the transverse direction (Batch 2). Up grinding can also produce quite high tensile residual stresses of 598 MPa with a depth of cut of 5 × 4 µm along the grinding direction. However, the scatter of the residual stress values is very large at higher depths of cut. An explanation for the large scatter might presumably be stronger strip deformations during grinding due to the low strip thicknesses in combination with the

higher depths of cut. More non-uniform electrochemically deposited initial states may contribute to the larger scatter of Batch 2 as well. In any case, the absolute values of the residual stresses along the grinding direction will always be greater than transverse to it.

Analyzes of microstructure show after grinding for all depths of cut in down and in up grinding a certain grain enlargement and micro strain reduction. So, during grinding, recovery and recrystallization processes must take place, which do not come to an end owing to the moderate microstructure changes. This requires corresponding temperature developments, which can be low for nc NiFe. Sufficiently high grinding temperatures develop most likely with larger depths of cut. As a result, down grinding with a depth of cut of 7×3 µm leads to maximum determined grain sizes of 23.4 nm and maximum decreases in micro strains to 0.41% as well as maximum residual stresses of 880 MPa. Furthermore, an increase in the lattice spacing during grinding is observed due to the onset of recrystallization and recovery processes.

Residual stress formation processes during grinding of nc metals must be largely comparable to those of microcrystalline metals. Like microcrystalline metals, nc nickel-iron should form compressive residual stresses on the workpiece surface primarily through cold plastic deformation. It can be assumed that increasing temperatures with increasing depth of cut reduce the mechanical effects and cause tensile residual stresses due to increasing dominance of the thermal effects with thermal-plastic deformation. Because of the high grain boundary energy of the nc microstructure, however, even small increases in temperature suffice for the onset of recovery and recrystallization processes. Recrystallization reduces the large grain boundary volumes of the original nc microstructure and thus the microstructure volume in the near-surface zone, which can shift the residual stresses toward absolutely more positive values.

In summary, it can be said that for very thin strip thicknesses, very careful grinding with a very small depth of cut of 20×1 µm enables reproducible good surface states and thickness dimensions with low scatter. Larger strip thicknesses can reduce the scatter and improve the reproducibility, as shown within initial investigations for thicknesses of 530 µm, even with slightly larger depths of cut. Depending on the grinding direction, surface structures with grooves parallel or perpendicular to the strips are possible. Different surface residual stresses with approximately the same surface roughness and the same microstructure can be realized by down or up grinding or, within limits, by varying the depth of cut. This makes it possible to perform fatigue tests on nc microsamples by considering the influence of machining residual stresses or the influence of surface grooves separately from the other surface states. The depth distributions of the residual stresses should also be taken into account for this task.

Acknowledgments: This publication was created thanks to funding from the University of Applied Sciences Kaiserslautern as part of students' final theses. The authors would like to thank the students who contributed to the present evaluations by their valuable help in carrying out the experiments. Particular mention should be made here of the master's thesis by Ms. Wenwen Du. Many thanks to Ms. Wenwen Du for the results. Special gratitude goes to the workshop of the University of Applied Sciences Kaiserslautern for carrying out various mechanical work and in particular for providing a surface grinding machine.
Author contributions: All the authors have accepted responsibility for the entire content of this submitted manuscript and approved submission.
Research funding: None declared.
Conflict of interest statement: The authors declare no conflicts of interest regarding this article.

References

[1] B. Scholtes and E. Macherauch, "Effects of the mechanical surface treatments on the strength properties of metallic materials," *Zeitschrift für Metallkunde*, vol. 77, no. 5, pp. 322–337, 1986.
[2] B. Scholtes, "Residual stresses introduced by machining," in *International Guidebook on Residual Stresses*, vol. 4, UK, Pergamon Press, 1987, pp. 59–71.
[3] E. Gassner and W. Schütz, *Evaluating Vital Vehicle Components by Programme Fatigue Tests*, London, FISITA-Congress, 1962, pp. 195–205.
[4] C. M. Sonsino, "Effect of lifetime under spectrum loading," *Mater. Test.*, vol. 52, nos. 7–8, pp. 440–451, 2010, https://doi.org/10.3139/120.110146.
[5] B. Syren, H. Wohlfahrt, and E. Macherauch, "The influence of residual stresses and surface topography on bending fatigue strength of machined CK 45 in different heat treatment conditions," in *International Conference on Mechanical Behavior of Materials*, Boston, Massachusetts, American Society of Metals, 1976, pp. 212–235.
[6] D. Löhe and J. E. Hoffmann, "Influence of macro residual stresses on the fatigue behavior of smooth and notched specimens made from a high strength steel," in *Advances in Surface Engineering*, Las Vegas, US, SAE Off-Highway Congress, 2002, pp. 75–81.
[7] D. Löhe, K.-H. Lang, and O. Vöhringer, "Residual stresses and fatigue behavior," in *Handbook of Residual stress and Deformation of Steel*, Materials Park, Ohio, US, ASM International, 2002, pp. 27–53.

[8] E. Macherauch, H. Wohlfahrt, and U. Wolfstieg, "Zur zweckmäßigen definition von Eigenspannungen," *HTM J. Heat Treat. Mater.*, vol. 28, no. 3, pp. 201–211, 1973, https://doi.org/10.1515/htm-1973-280305.

[9] E. Macherauch, "Introduction to residual stress," in *International Guidebook on Residual Stresses*, vol. 4, UK, Pergamon Press, 1987, pp. 1–36.

[10] E. Siebel and M. Gaier, "Untersuchungen über den Einfluss der Oberflächenbeschaffenheit auf die Dauerschwingfestigkeit metallischer Bauteile," *Verein Deutscher Ingenieure, VDI-Zeitschrift*, vol. 98, no. 30, pp. 1715–1723, 1956.

[11] E. Brinksmeier and B. Karpuschewski, "Prozessnahe Überwachung des Eigenspannungszustands geschliffener Werkstücke mit magnetischen Verfahren," in *Residual Stresses*, Oberursel, DGM Infomationsgesellschaft, 1993, pp. 863–872.

[12] H. K. Tönshoff, T. Friemuth, and J. C. Becker, "Process monitoring in grinding," in *52nd General Assembly of CIRP*, ES, San Sebastian, 2002, pp. 551–571.

[13] B. Syren, H. Wohlfahrt, and E. Macherauch, "On the generation of residual machining stresses," *Archiv Eisenhüttenwesen*, vol. 48, no. 8, pp. 421–426, 1977, in German, Zur Entstehung von Bearbeitungseigenspannungen, https://doi.org/10.1002/srin.197705039.

[14] B. Syren, *Der Einfluss spanender Bearbeitung auf das Biegewechselverformungsverhalten von Ck 45 in verschiedenen Wärmebehandlungszuständen*, Dissertation, Germany, University of Karlsruhe, 1975.

[15] J. E. Hoffmann, *Der Einfluss fertigungsbedingter Eigenspannungen auf das Biegewechselverhalten von glatten und gekerbten Proben aus Ck 45 in verschiedenen Werkstoffzuständen*, Dissertation, Germany, University of Karlsruhe, 1984.

[16] W. Ding, L. Zhang, Z. Li, Y. Zhu, H. Su, and J. Xu, "Review on grinding-induced residual stresses in metallic materials," *Int. J. Adv. Manuf. Technol.*, vol. 88, nos. 9–12, pp. 2939–2968, 2017, https://doi.org/10.1007/s00170-016-8998-1.

[17] K. Ji, X. Zhang, S. Yang, L. Shi, S. Wang, and Y. Wu, "Surface integrity of quenched steel 1045 machined by CBN grinding wheel and SiC grinding wheel," *Int. J. Mater. Struct. Integr.*, vol. 8, no. 2, pp. 179–187, 2017, https://doi.org/10.1108/IJSI-03-2016-0011.

[18] Z. Pala and N. Ganev, "X-ray diffraction study of anisotropic state of residual stress after down-cut and up-cut face grinding," *Powder Diffr.*, vol. 24, no. 2, pp. 1–3, 2009, https://doi.org/10.1154/1.3120606.

[19] T. Tawakoli and S. J. Tavakkoli, "Hochleistungsschleifen (HEDG) von Inconel und anderen Werkstoffen," *VDI-Zeitschrift*, vol. 134, no. 1, pp. 48–57, 1992.

[20] M. J. Balart, A. Bounzina, L. Edwards, and M. E. Fitzpatrick, "The onset of tensile residual stresses in grinding of hardened steels," *Mater. Sci. Eng., A*, vol. 367, pp. 132–142, 2004, https://doi.org/10.1016/j.msea.2003.10.239.

[21] J. E. Hoffmann and H. Clemens, "Kerbfertigung und Kerbschlagbiegeverhalten," *Fortschritts-Berichte VDI, Reihe*, vol. 5, no. 687, 2003.

[22] J. E. Hoffmann and H. Clemens, "X-ray stress and residual stress analysis of charpy steel specimens," *Mater. Test.*, vol. 49, nos. 11–12, pp. 588–595, 2007, https://doi.org/10.3139/120.100851.

[23] Q. Zeng, G. Liu, L. Liu, and Y. Qin, "Investigation into grindability of a superalloy and effects of grinding parameters on its surface integrity," *Proc. IME B J. Eng. Manufact.*, vol. 229, no. 2, pp. 238–250, 2015, https://doi.org/10.1177/0954405414526384.

[24] X. P. Xu, Y. Q. Yu, and H. J. Xu, "Effect of grinding temperatures on the surface integrity of a nickel-based superalloy," *J. Mater. Process. Technol.*, vol. 129, nos. 1–3, pp. 359–363, 2002, https://doi.org/10.1016/S0924-0136(02)00656-8.

[25] W. Österle, P. X. Li, and G. Nolze, "Influence of surface finishing on residual stress depth profiles of a coarse-grained nickel-base superalloy," *Mater. Sci. Eng., A*, vol. 262, nos. 1–2, pp. 308–311, 1999, https://doi.org/10.1016/S0921-5093(98)01018-1.

[26] R. Schwaiger, J.-T. Reszat, K. Bade, J. Aktaa, and O. Kraft, "A combined microtensile testing and nanoindentation study of the mechanical behavior of nanocrystallinw LIGA Ni-Fe," *Int. J. Mater. Res.*, vol. 100, no. 1, pp. 68–75, 2009, https://doi.org/10.3139/146.101785.

[27] Y. Marita and I. I. Yaacob, "Structural characterization of electrodeposited nickel-iron alloy films," *Mater. Sci. Forum*, vols. 654–656, pp. 2430–2433, 2010, part 3, https://doi.org/10.4028/www.scientific.net/MSF.654-656.2430.

[28] D. P. Arnold, M. Saumer, and Y.-K. Yoon, "Additive processes in metals," in *MEMS Materials and Processes Handbook*, New York, Springer Science-Business Media, LLC, 2011, pp. 137–191.

[29] R. Slatter and R. Degen, "The micro harmonic drive: a high precision gear system miniaturized by direct-LIG," in *Proc. of the 4th Euspen International Conference*, Glasgow, Scotland, 2004, pp. 13–14.

[30] M. Dao, L. Lu, R. J. Asaro, J. T. M. De Hosson, and E. Ma, "Toward a quantitative understanding of mechanical behavior of nanocrystalline metals," *Acta Mater.*, vol. 55, no. 12, pp. 4041–4065, 2007, https://doi.org/10.1016/j.actamat.2007.01.038.

[31] B. L. Boyce and H. A. Padilla, II, "Anomalous fatigue behavior and fatigue-induced grain growth in nanocrystalline nickel alloys," *Metall. Mater. Trans.*, vol. 42, no. 7, pp. 1793–1804, 2011, https://doi.org/10.1007/s11661-011-0708-x.

[32] M.-T. Schmitt, *Charakterisierung galvanisch hergestellter nanokristalliner Nickel-Eisen-Legierungen*, Dissertation, Germany, TU Kaiserslautern, 2014.

[33] J. E. Hoffmann, M.-T. Schmitt, D. Eifler, T. Beck, P. Klär, and M. Saumer, "Bending deformation and indentation hardness of electrochemical deposited nanocrystalline nickel-iron alloys," *Mater. Test.*, vol. 60, no. 11, pp. 1041–1049, 2018, https://doi.org/10.3139/120.111259.

[34] A. M. Rashidi and A. Amadeh, "The effect of current density on the grain size of electrodeposited nanocrystalline nickel coatings," *Surf. Coat. Technol.*, vol. 202, no. 16, pp. 3772–3776, 2008, https://doi.org/10.1016/j.surfcoat.2008.01.018.

[35] A. M. Rashidi and A. Amadeh, "The effect of saccharin addition and bath temperature on the grain size of nanocrystalline nickel coatings," *Surf. Coat. Technol.*, vol. 204, no. 3, pp. 353–358, 2009, https://doi.org/10.1016/j.surfcoat.2009.07.036.

[36] F. Giro, K. Bedner, C. Dhum et al, "Pulsed electrodeposition of high aspect-ratio NiFe assemblies and its influence on spatial alloy composition," *Microsyst. Technol.*, vol. 14, no. 8, pp. 1111–1115, 2008, https://doi.org/10.1007/s00542-008-0614-3.

[37] C. Cheung, F. Djuanda, U. Erb, and G. Palumbo, "Electrodeposition of nanocrystalline Ni-Fe alloys," *Nanostruct.*

Mater., vol. 5, no. 5, pp. 513–523, 1995, https://doi.org/10.1016/0965-9773(95)00264-F.

[38] H. Li and F. Ebrahimi, "Synthesis and characterization of electrodeposited nanocrystalline nickel-iron alloys," *Mater. Sci. Eng., A*, vol. 347, nos. 1–2, pp. 93–101, 2003, https://doi.org/10.1016/S0921-5093(02)00586-5.

[39] A. M. El-Sherik and U. Erb, "Synthesis of bulk nanocrystalline nickel by pulsed electrodeposition," *J. Mater. Sci.*, vol. 30, no. 22, pp. 5743–5749, 1995, https://doi.org/10.1007/BF00356715.

[40] A. M. Pillai, A. Rajendra, and A. K. Sharma, "Pulse electrodeposition of nanocrystalline nickel on AA 6061 for space applications," *Trans. Inst. Met. Finish.*, vol. 90, no. 1, pp. 44–51, 2012, https://doi.org/10.1179/174591911X13165161228286.

[41] U. Kirsch, *Elektrochemische Abscheidung von spannungsarmen Nickel-Eisen-Legierungsschichten und ihre Eigenschaften für Bauteile der Mikrosystemtechnik*, Dissertation, Freiburg, Germany, Albert-Ludwig-Universität, 2000.

[42] J. E. Hoffmann, K. Bedner, H. Clemens et al, "The influence of electroplating parameters on the conditions of deposited nickel-iron coatings," *Mater. Werkst.*, vol. 39, no. 3, pp. 209–216, 2008, https://doi.org/10.1002/mawe.200800286.

[43] K. Schüler, B. Philippi, M. Weinmann, V. M. Marx, and H. Vehoff, "Effects of processing on texture, internal stresses and mechanical properties during the pulsed electrodeposition of nanocrystalline and ultrafine-grained nickel," *Acta Mater.*, vol. 61, no. 11, pp. 3945–3955, 2013, https://doi.org/10.1016/j.actamat.2013.03.008.

[44] J.-G. Hong and C.-Y. Lee, "Development of a real-time measurement device for monitoring the internal stress during electroplating," *Exp. Tech.*, vol. 41, no. 1, pp. 51–57, 2017, https://doi.org/10.1007/s-40799-016-0155-0.

[45] F. Czerwinski, "Grain size-internal stress relationship in iron-nickel alloy electrodeposits," *J. Electrochem. Soc.*, vol. 143, no. 10, pp. 3327–3332, 1996, https://doi.org/10.1149/1.1837206.

[46] F. Czerwinski and Z. Kedzierski, "On the mechanism of microcrack formation in nanocrystalline Fe-Ni electrodeposits," *J. Mater. Sci.*, vol. 32, no. 11, pp. 2957–2961, 1997, https://doi.org/10.1023/A:1018693005002.

[47] M. Schlesinger and M. Paunovic, *Modern Electroplating*, 4th ed., The Electrochemical Society, New York, Wiley and Sons, 2001.

[48] A. M. El-Sherik, J. Shirokoff, and U. Erb, "Stress measurements in nanocrystalline Ni electrodposits," *J. Alloys Compd.*, vol. 389, nos. 1–2, pp. 140–143, 2005, https://doi.org/10.1016/j.jallcom.2004.08.010.

[49] Y. Woo and S.-H. Kim, "Sensitivity analysis of plating conditions on mechanical properties of thin film for MEMS applications," *J. Mech. Sci. Technol.*, vol. 25, no. 4, pp. 1017–1022, 2011, https://doi.org/10.1007/s12206-011-0205-6.

[50] J. D. Giallonardo, U. Erb, G. Palumbo, G. A. Botton, and C. Andrei, "Internal stresses in nanocrystalline nickel & nickel-iron alloys," *Mater. Sci. Forum*, vols. 706–709, pp. 1607–1611, 2012, https://doi.org/10.4028/www.scientific.net/MSF.706-709.1607.

[51] E. Wagner, "Zur Ermittlung der Abscheidungseigenspannungen und verbleibenden Eigenspannungen in galvanisch hergestellten Nickelschichten nach der Spiralkontraktometer- und Streifendehnungs-Methode," *J. Mater. Technol.*, vol. 6, no. 3, pp. 95–108, 1975, https://doi.org/10.1002/mawe.19750060305.

[52] V. C. Nguyen, C. Y. Lee, L. Chang, F. J. Chen, and C. S. Lin, "The relationship between nano crystallite structure and internal stress in Ni coatings electrodeposited by Watts bath electrolyte mixed with supercritical CO_2," *J. Electrochem. Soc.*, vol. 159, no. 6, pp. D393–D399, 2012.

[53] C.-Y. Lee, K.-H. Lee, and B.-W. Wang, "Nickel electroplating in post supercritical CO_2 mixed Watts bath under different agitations," *Int. J. Mech. Eng. Mechatron.*, vol. 11, no. 7, pp. 1319–1325, 2017, https://doi.org/10.5281/zenodo.1131322.

[54] N. Pangarov and R. Pangarova, "Stress in electrodeposited metals general thermodynamik theory," *J. Electroanal. Chem. Interfacial Electrochem.*, vol. 91, no. 2, pp. 173–188, 1978, https://doi.org/10.1016/S0022-0728(78)80098-9.

[55] G. Richardson and B. Stein, "Comparative study of three internal stress measurement methods," in *Electroforming Course and Symposium*, San Diego, CA, USA, American Electroplaters and Surface Finishers Society, 1998, pp. 21–30.

[56] G. Sotirova-Chakarova and S. Armyanov, "Innere spannungen in galvanischen Überzügen Teil 1," *Electroplat. Technol.*, vol. 81, no. 6, pp. 2004–2013, 1990.

[57] E. Macherauch and P. Müller, "Das $\sin^2\psi$-Verfahren der röntgenographischen Spannungsmessung," *Z. Angew. Phys.*, vol. 13, no. 7, pp. 305–312, 1961.

[58] K. van Acker, L. de Buyser, J. P. Celis, and P. van Houtte, "Characterization of thin nickel electrocoatings by low-incident-beam-angle diffraction method," *J. Appl. Crystallogr.*, vol. 27, no. 1, pp. 56–66, 1994, https://doi.org/10.1107/S002188989300651X.

[59] R. Naumann, "Eigenspannungen in galvanisch abgeschiedenen Schichten," *HTM J. Heat Treat. Mater.*, pp. 106–112, 1982, Beiheft.

[60] H. A. Padilla and B. L. Boyce, "A review of fatigue behavior in nanocrystalline metals," *Exp. Mech.*, vol. 50, no. 1, pp. 5–23, 2010, https://doi.org/10.1007/s11340-009-9301-2.

[61] K. Dai and L. Shaw, "Analysis of fatigue resistance improvements via surface severe plastic deformation," *Int. J. Fatig.*, vol. 30, no. 8, pp. 1398–1408, 2008, https://doi.org/10.1016/j.ijfatigue.2007.10.010.

[62] T. Ungár, I. Dragomir, A. Révész, and Á. Borbély, "The contrast factors of dislocations in cubic crystals: the dislocation model of strain anisotropy in practice," *J. Appl. Cryst.*, vol. 32, no. 5, pp. 992–1002, 1999, https://doi.org/10.1107/S0021889899009334.

[63] V. Valvoda and M. Järvinen, "On the Harris texture index," *Powder Diffr.*, vol. 5, pp. 200–203, 1990, https://doi.org/10.1017/S0885715600015797.

[64] PCPDFWIN, *JCPDS International Centre for Diffraction Data*, Newtown Square, PA, USA, 2003, V 2.6.

[65] B. Eigenmann and E. Macherauch, "Röntgenographische Untersuchung von Spannungszuständen in Werkstoffen, Teil III," *Mater. Werkst.*, vol. 27, no. 9, pp. 426–437, 1996, https://doi.org/10.1002/mawe.19960270907.

[66] U. Klement, U. Erb, A. M. El-Sherik, and K. T. Aust, "Thermal stability of nanocrystalline Ni," *Mater. Sci. Eng., A*, vol. 203, nos. 1–2, pp. 177–186, 1995, https://doi.org/10.1016/0921-5093(95)09864-X.

[67] H. Q. Li and F. Ebrahimi, "An investigation of thermal stability and microhardness of electrodeposited nanocrystalline nickel-21 % iron alloys," *Acta Mater.*, vol. 51, no. 13, pp. 3905–3913, 2003, https://doi.org/10.1016/S1359-6454(03)00215-5.
[68] J. E. Hoffmann, M.-T. Schmitt, D. Eifler et al, "Mechanical behavior of annealed electrochemically deposited nanocrystalline nickel-iron alloys," *Mater. Test.*, vol. 62, no. 3, pp. 225–241, 2020, https://doi.org/10.3139/120.111475.
[69] H. S. Kim, Y. Estrin, and M. B. Bush, "Plastic deformation behaviour of fine-grained materials," *Acta Mater.*, vol. 48, no. 2, pp. 493–504, 2000, https://doi.org/10.1016/S1359-6454(99)00353-5.
[70] Y. M. Wang, S. Cheng, Q. M. Wei, E. Ma, T. G. Nieh, and A. Hamza, "Effects of annealing and impurities on tensile properties of electrodeposited nanocrystalline Ni," *Scr. Mater.*, vol. 51, no. 11, pp. 1023–1028, 2004, https://doi.org/10.1016/j.scriptamat.2004.08.015.
[71] F. Ebrahimi and H. Li, "The effect of annealing on deformation and fracture of a nanocrystalline fcc metal," *J. Mater. Sci.*, vol. 42, no. 5, pp. 1444–1454, 2007, https://doi.org/10.1007/s10853-006-0969-8.
[72] N. Dong, C. Zhang, J. Li, and P. Han, "Synthesis and thermal stability of nanocrystalline nickel coatings by direct current electrodeposition," *Rare Met. Mater. Eng.*, vol. 45, no. 4, pp. 885–888, 2016, https://doi.org/10.1016/S1875-5372(16)30093-5.

The authors of this contribution

Joachim E. Hoffmann
Prof. Dr.-Ing. Joachim E. Hoffmann, born in 1953, studied Mechanical Engineering at the University of Karlsruhe, Germany, from 1975 to 1979. From 1979 to 1984, he studied and received his Doctorate at the Institute for Materials Science I. 1985 to 1988 he worked as a group leader on the development of electronic fuel pumps at the company Robert Bosch GmbH in Stuttgart, Germany. In 1988, he was appointed to Chair at the University of Applied Sciences Kaiserslautern, Germany, in the Department of Materials Science and has been professor emeritus since 2018.

Vrushali Pawar
Vrushali Pawar, born in 1990, received Bachelors of Engineering Degree in Mechanical Engineering VIT, Pune, India, in 2008 and Masters of Engineering Degree in Mechanical Engineering from University of Applied Sciences Kaiserslautern, in 2018. During Masters study, she completed research study which interests in surface states by grinding Nanocrystalline Nickel-Iron. She has gained over 5 years of experience leveraging in depth knowledge of Manufacturing process planning while working at John Deere factories in India & Germany. Currently, she is working as Manufacturing Engineer at John Deere Zweibrücken and responsible for Assembly & Welding process planning for Harvester Product line.

Dietmar Eifler
Prof. Dr.-Ing. habil. Dietmar Eifler, born in 1949, received his PhD at the University of Karlsruhe. From 1991 to 1994 he was Professor at the University of Essen. From 1994 until 2015 he was Professor and from 2015 to 2017 Senior Research Professor at the Institute of Materials Science and Engineering at the Technical University of Kaiserslautern. His research activities are focused on the microstructure-based characterization of the fatigue behavior of metallic materials using mechanical, electrical, magnetic, acoustic as well as thermal measuring techniques in the LCF-, HCF- and VHCF-regime.

Tina Eyrisch
Dr.-Ing. Tina Eyrisch, born in 1978, studied Mechanical Engineering at the Technical University of Kaiserslautern, Germany. In 2004, she became a Research Assistant at the Institute for Manufacturing Technology and Production Systems (FBK) at the Technical University of Kaiserslautern, Germany. She received her Doctoral degree in Engineering, in 2009. From 2011 to 2014, she was a Junior Professor in the field of Cutting at FBK. She is currently working as a visiting scientist at the Institute for Quality, Modeling, Manufacturing, and Materials (QM3) at the University of Applied Sciences Kaiserslautern (Hochschule Kaiserslautern). She concentrates on the machinability of metallic and non-metallic materials and technical cleanliness.

Torsten Hielscher
Prof. Dr.-Ing. Torsten Hielscher, born in 1977, studied Industrial Engineering at the Technical University of Kaiserslautern, Germany. From 2003 to 2008 he worked as a Research Assistant at the Institute for Manufacturing Technology and Production Systems (FBK) at the Technical University of Kaiserslautern, Germany. He received his Doctoral degree in Engineering, in 2008. From 2005 to 2008, he headed the research group "Manufacturing Technology" at FBK. Afterwards, he worked at Schaeffler Technologies AG in Homburg, Germany, as Head of the Department for Manufacturing Technologies and Process Engineering. Since 2012, he has been Professor in the field of Production and Manufacturing Technology at the University of Applied Sciences Kaiserslautern (Hochschule Kaiserslautern), Germany. He is a founding member of the Institute for Quality, Modeling, Manufacturing, and Materials (QM³), which was established in 2019 at the University of Applied Sciences Kaiserslautern. His research focuses on the control and optimization of manufacturing process chains. There, he mainly deals with cutting processes with geometrically defined cutting edges, especially with respect to chip and burr formation as well as technical surfaces.

Monika Saumer
Prof. Dr. rer. nat. Monika Saumer was born in 1961. She graduated in Chemistry at the University in Bonn, Germany. After her PhD in Analytical Chemistry at the University of Karlsruhe, Germany, she worked at the Forschungszentrum Karlsruhe (now: Karlsruhe Institute of Technology = KIT) in the Institute of Microstructuring Technology. In 1998 she obtained a Professorship at the University of Applied Sciences Kaiserslautern/Zweibrücken. Her research activities are focused on chemical processes for microfabrication including the electroplating of alloys, nanostructuring and related characterization methods.

Patrick Klär
Prof. Dr.-Ing. Patrick Klär, born in 1965, studied Material Sciences at The University of Saarland, Germany, from 1986 to 1991. Thereafter, he worked as a Scientific Assistant for nonlinear modeling and finite element simulations at the Chair of the Technical Mechanics at the University of Saarland and received his PhD degree in 1995. Subsequently, he worked as Deputy Head of the Development and Quality Assurance Department for a subsidiary company of the Saarstahl AG. From 1999 to 2000, he was Operating Chief for hard materials manufacturing at the subsidiary company of the Saarstahl

AG. Since February 2000, he has been Professor for design and simulation of microsystems at the University of Applied Sciences Kaiserslautern. His working group works on the field of design and finite element simulation of microsystems and on the field of micro-cutting of microsystem materials and components.

Martin-Tobias Schmitt
Dr.-Ing. Martin-Tobias Schmitt, born in 1971, studied Mechanical Engineering at University of Applied Science in Kaiserslautern, Germany, where he completed his Dipl.-Ing. (FH) in 1999. After several years in industry, he started basic research at the University of Applied Sciences in Kaiserslautern. In 2014, he received his Dr.-Ing. degree from the Technical University of Kaiserslautern. Since 2014, he works for the Voestalpine Böhler Welding Fontargen GmbH as Manager Global R&D Brazing.

Peter Starke
Prof. Dr.-Ing. habil. Peter Starke, born in 1977, studied Mechanical Engineering at the Technical University of Kaiserslautern, Germany. Since 2002, he has been a research assistant at the Institute of Materials Science and Engineering (WKK) at the Technical University of Kaiserslautern, Germany. He received his Doctoral degree in Engineering in 2007 working on “The fatigue life calculation of metallic materials under constant amplitude loading and service loading”. From 2007 to 2012, he headed the research group “Fatigue life calculation” at WKK. Afterwards, he changed to Fraunhofer IZFP in Saarbrücken, Germany. From 2013 to 2018, he was a Senior Research Associate for the Chair of Non-Destructive Testing and Quality Assurance at Saarland University in Saarbrücken, Germany. In 2018, he became a Professor in the field of Materials Science and Materials Testing at the University of Applied Sciences Kaiserslautern (Hochschule Kaiserslautern). His research is mainly focused on the use of non-destructive measurement techniques for the characterization of fatigue behavior and the fatigue life calculation of metallic and non-metallic materials in the LCF-, HCF- and VHCF-regime as well as for the evaluation of defects and inhomogeneities in the materials microstructure.